Relationship between weathering, elemental Sulfur Formation and Sulphide Self-heating

Kowoon Park

Department of Mining and Materials Engineering

McGill University

Montreal, Canada

March 2015

A thesis submitted to McGill University

in partial fulfillment of the requirements of the degree of

Master of Engineering

Abstract

Some sulphides have a propensity to self-heat that under certain conditions can lead to hazardous environments, from noxious gas emission (SO_2) to sulfide ignition. Self-heating results from oxidation that appears to proceed through three distinct stages: stage A (below 100°C) associated with production of elemental sulfur, stage B (above 100°C) which involves oxidation of the sulfur, and stage C (above 350°C), the direct oxidation of the sulfide (ignition) which is independent of the oxidation history of the sample.

Elemental sulfur is one of the oxidation products known to form in stage A that fuels the self-heating in stage B. In the first part of this thesis, the relationship between elemental sulfur formation in stage A , and the self-heating in stage B was investigated through the use of the self-heating apparatus. Two site-specific samples were tested under different stage A conditions, and then tested at stage B. It was generally observed that increasing the temperature and the duration of stage A increased the formation of elemental sulfur which correlated with increased self-heating in stage B. Exceptions were observed with the samples tested at high stage A temperatures (55~70°C); the set air flow rate (100mL/min) seemed insufficient for the samples to fully oxidize.

Samples showed re-activation when repeatedly tested and continued to heat until all fuel was exhausted. The second part of the thesis then investigated the total heat that a sample can generate, along with the cumulative elemental sulfur

produced. Reaction products of self-heating were identified at the completion of the repeated tests by a combination of analytical techniques. Results showed that the elemental sulfur formed from each cycle correlated well with the self-heating in stage B; however, the cumulative sulfur was not directly proportional to the total heat produced by the sample. Pyrrhotite was identified as the ultimate source of the reactions, generating goethite and iron sulphates as final reaction products.

Résumé

Certains sulfures ont une propension à l'auto-échauffement faisant en sorte que dans certaines conditions cela peut mener à des environnements dangereux, allant de l'émission de gaz nocifs (SO2) à l'ignition de sulfure. Les résultats de l'auto-échauffement provenant de l'oxydation semblent passer par trois étapes distinctes: l'étape A (moins de 100^0 C) associée à la production de soufre élémentaire, le stade B (plus de 100^0 C) qui implique l'oxydation du soufre, et le stade C (plus de 350^0 C), l'oxydation directe du sulfure (ignition) qui est indépendante des antécédents de l'oxydation de l'échantillon.

Le soufre élémentaire est l'un des produits d'oxydation connus pour former au stade A ce qui alimente l'auto-échauffement au stade B. Dans la première partie de cette thèse, la relation entre la formation de soufre élémentaire au stade A, et l'auto-échauffement au stade B a été étudiée grâce à l'utilisation de l'appareil d'auto-échauffement. Deux échantillons spécifiques au site ont été testés dans différentes conditions de stade A, et ont ensuite été testés à l'étape B. On a généralement observé que l'augmentation de la température et de la durée de l'étape A ont augmenté la formation de soufre élémentaire ce qui est corrélé par une augmentation de l'auto-chauffage dans l'étape B . Des exceptions ont été observées avec les échantillons testés à des températures du stade A (55~70°C); le débit d'air (100 ml/min) paraissait insuffisant pour que les échantillons s'oxydent complètement.

Les échantillons ont montré une réactivation lorsqu'ils ont été testés à plusieurs reprises et ont continué à s'échauffer jusqu'à ce que tout le carburant ait été épuisé. La deuxième partie de la thèse a ensuite examiné la chaleur totale qu'un échantillon peut générer, ainsi que le soufre élémentaire cumulatif produit. Des produits de réaction de l'auto-échauffement ont été identifiés à la fin des tests répétés par une combinaison de techniques analytiques. Les résultats ont montré que le soufre élémentaire formé à partir de chaque cycle est bien corrélé par l'auto-échauffement dans l'étape B; toutefois, le soufre cumulatif n'est pas directement proportionnel à la chaleur totale produite par l'échantillon. La pyrrhotine a été identifiée comme la source ultime des réactions, générant de la goethite et des sulfates de fer comme produits finaux de la réaction.

Acknowledgments

I would like to first thank my Creator, Lord and Saviour Jesus Christ, for forgiving me from all my sins and adopting me into His family.

I also would like to thank the following people for their help and support during the years at McGill University:

Professor James A. Finch, thank you for the wonderful opportunity under your supervision, for the discussions, advice and patience.

Mr. Frank Rosenblum, thank you for believing me with patience, for giving me motivations, encouragements, and all the help through the years.

Jan Nesset and Sarah Jung, thank you for the discussions and ideas.

Ray Langlois, thank you for your kindness, for all the trainings and help in the laboratory.

Monique Riendeau, Lihong Shang, Lang Shi and Ranjan Roy, thank you for all the trainings and technical support.

Ravinder Multani, Amir Mohammad Nazari , Gul Zeb, Dong-Geun Kim, Sun Young Park and Sung Jae Moon, thank you for your help in analysis of data.

NSERC and the Chair Sponsors (Vale, Teck, Xstrata Process Support, Shell Canada, Barrick Gold, SGS Lakefield Research, COREM and Flottec), thank you for your financial support.

Everyone in Mineral processing group, thank you for your friendship, encouragement and support.

All my brothers and sisters in Christ, thank you for providing me with lots of love and encouragement

Table of Contents

List of Figures

List of Tables

1 Introduction

1.1 Self-heating of Sulfides

1.1.1 Problem Statement

Over the years there have been numerous reports of underground fires caused by self-heating. Overwhelmingly, coal has been a major source of underground fires [1-3]; however, sulfide mineral self-heating also gives rise to such consequences both underground and aboveground [4-8].

Some sulfides – especially pyrrhotite [4, 9-11] – have shown to be a major contributor to self-heating that leads to creation of hazardous environments [12] (toxic gas, depletion of oxygen, etc.) and, in some extreme cases, creation of fires and loss of life [4, 7]. As the sulfides undergo the stages of mineral processing – such as blasting, crushing, milling, etc. – they are exposed to environmental conditions that allow for oxidation, that can result in self-heating [4, 5, 13, 14]. Incidents associated with the self-heating of sulfides are well documented [4-8].

Dealing with the effects of sulfide self-heating has been a costly and disruptive process in the mining industry. Some research in this topic has shown that a variety of mitigation methods can in part alleviate the negative effects of self-heating [4, 5, 9, 10, 15-18]. These methods however are not always practical, or entirely effective [5, 9, 16, 17, 19]. By having a better understanding of the

reactions leading to self-heating, it is expected that a better and more effective mitigation method can be developed.

1.1.2 Process of Self-heating of Sulfides

The self-heating of sulfides proceeds through three stages, namely stages A, B and C [9, 17]:

Stage A: the material is moist (1-15%), and its temperature is below 100^0C.

Stage B: the material is dry, and its temperature is above 100^0C but below 400^0C.

Stage C: the material is dry, and its temperature exceeds 400^0C.

In each of the above stages, the heat generated is primarily a result of exothermic oxidation reactions.

In stage A, the sulfides oxidize to form elemental sulfur [9, 17, 20] and other oxidation products [10, 11, 21]. The reactions are exothermic, generating self-heating. Elevated ambient temperature and high relative humidity promote the oxidation reactions [5]. The predominant reaction in this stage is shown in Equation 1.1, where FeS represents pyrrhotite.

$$4FeS + 3O_2 + 2H_2O \rightarrow 4FeO{\cdot}OH + 4S \qquad (1.1)$$

Reaction 1.1 is also accompanied by acid formation, as described Sections 2.3.1.1 and 2.3.2.1.

In stage B, the elemental sulfur generated in stage A oxidizes to form SO_2 gas and in the process generates additional heating [9, 17, 20]. The reaction is shown in Equation 1.2.

$$S + O_2 \rightarrow SO_2 \quad (1.2)$$

In stage C, the temperature is high enough that the sulfides oxidize directly. This stage is sometimes referred to as ignition, roasting or runaway temperature [17, 20]; the heating rates in stage C are substantially higher than the heating rates in either of the previous two stages.

1.1.2.1 Interrelation among stages A, B and C

As stated, the self-heating in stage A results from the oxidation of sulfides to generate a fuel (elemental sulfur) which drives the reaction in stage B; that is, the self-heating in stage B is contingent on what transpired in stage A. In contrast, the self-heating in stage C is independent of what transpired in stages A or B [20], the remaining sulfides reacting directly.

This present work focuses on the interrelationship between stages A and B; stage C is not considered.

1.1.2.2 Oxidation in stage A

The oxidation in stage A is also termed weathering. The extent of weathering is contingent on many factors, such as the ambient temperature [9, 22, 23], relative humidity[4, 15], oxygen content [9, 24], exposure time [20]. The

weathering process will therefore affect the amount of elemental sulfur formed in stage A, thus the magnitude and duration of self-heating in stage B.

1.1.3 Characteristics of Sulfides

1.1.3.1 Delay on the onset of self-heating

Tests have shown that some sulfides exhibit a delay on the onset of self-heating, i.e., there is very little, or no self-heating at the start of the test (oxidation), however, as the test progresses the sample becomes active and exhibits self-heating. This delay, also referred to as the induction period, may result from a buffering action by minerals which inhibits acid formation and thus blocks Reaction 1.1 [22, 25]; it is believed that when the capacity of the buffering minerals is exhausted, the moisture pH drops and increases the rate of oxidation [26, 27] thus affecting self-heating. Temperature, acidity and the amount of oxidative products formed on the material surface are some of the factors affecting the length of the delay [10, 27]. The acid-generating reactions are discussed in further detail in Sections 2.3.1.1 and 2.3.2.1.

1.1.3.2 Total Potential Heat

Tests have also shown that, after a material has undergone a stage A followed by stage B testing to exhaustion (i.e., no more self-heating is produced) it can re-generate self-heating upon re-moisturizing and re-testing [17]. The series of the tests can be continued until the sample ceases to exhibit any self-heating in

either of the two stages. The amount of heat generated from each stage is recorded and accumulated through the series of tests; this value, referred to as the heat generating capacity, defines the total amount of heat that a material can possibly generate. Further details are discussed in Section 3.3.3.

1.2 Objectives

The objectives of this thesis are:

- To determine the effect of weathering in stage A on the generation of elemental sulfur and the resulting self-heating in stage B.
- To determine the total potential heat that a given material can generate.
- To determine the reaction products of self-heating of pyrrhotite through the use of XRD and XPS as step to identifying the reaction pathway(s).

1.3 Organization

This thesis consists of six Chapters. Chapter one introduces the self-heating of sulfides, along with the objectives of the research. Chapter two is a literature review organized into three sections: (1) measurement methods, (2) causes and mitigations and (3) oxidation reactions of sulfide self-heating. Chapter three describes the experimental work conducted for the thesis, followed by the results summarized in Chapter four and discussion in Chapter five. The conclusions and recommendations are presented in Chapter six.

2 Literature Review

2.1 Self-heating Measurement methods

A number of self-heating measurement methods have been developed over the years to measure the potential hazards associated with sulphides. Based on different theories, these methods test self-heating characteristics of sulphides under different conditions and over different scales.

2.1.1 Furnace Tube Measurements

A combustion test apparatus (Figure 2-1) created by Good [4] is used to determine the ignition temperatures (stage C) of minus-200-mesh sulphides. The sulphide sample contained in a porcelain container is continuously heated up to ignition and SO_2 emission is continuously monitored (Figure 2-2). Good determined ignition temperatures of the sulphides tested samples to be in the range 205°C to 515°C, with most of the samples in the range 385°C to 450°C. Samples with low ignition temperature were considered more reactive, and were investigated further.

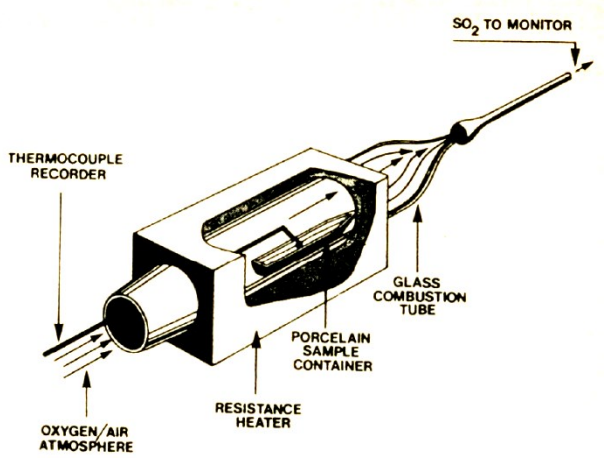

Figure 2-1: Combustion Test Apparatus

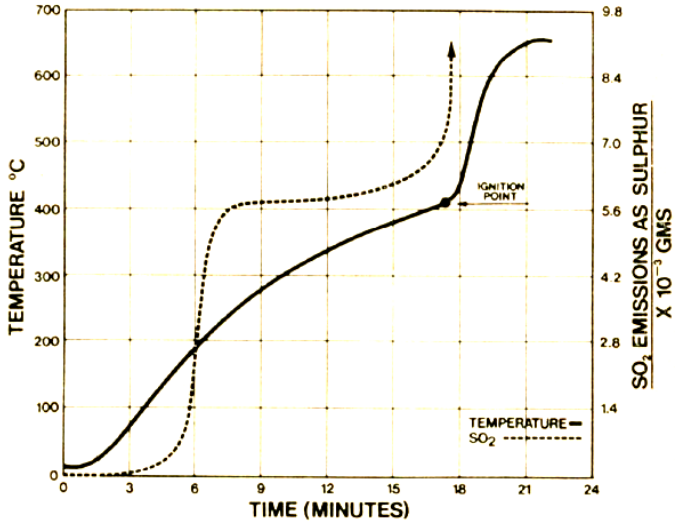

Figure 2-2: Typical heating Curve and SO_2 Emissions

A drop tube furnace, similar to Good's combustion test apparatus, is used to measure the ignition temperatures of spontaneously combustible materials, including sulphides [28]. Constructed as a vertical furnace with a sample tube inside, oxidation proceeds as the sample is subjected to the test conditions; the degree of oxidation is measured by the analysing the exit gas.

2.1.2 Differential Scanning Calorimetry (DSC)

A DSC, coupled with Advanced Thermo Kinetic Software (AKTS) was used by Iliyas *et al*. to investigate the self-heating behavior of sulphide ores [29-31]. Samples weighing about 10 mg are subjected to a continuous heating, with air provided at a steady flow rate of 10mL/min; typical results of active sulphide samples are shown in Figure 2-3 [30], tested at different heating rates (0.5, 1, 3 and 5 K/min). Parameters such as reaction rates and activation energies are calculated using the AKTS software; the values are then used to predict the behaviour of the samples subjected to different conditions.

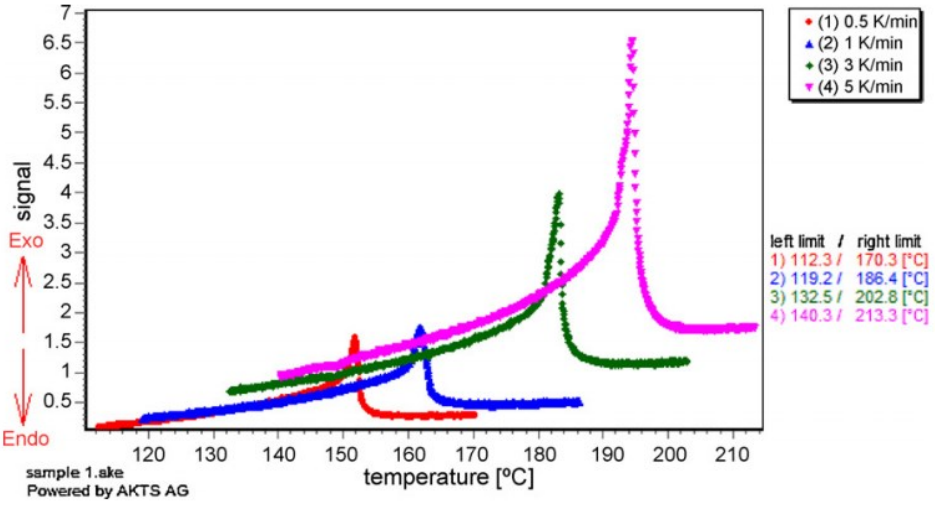

Figure 2-3: DSC Curves of Sulphide Mineral Samples

2.1.3 Hot-Storage Methods

2.1.3.1 Original Hot-Storage Method

The hot-storage method uses the Frank-Kamenetskii [32] mathematical model to assess the self-heating risk of many materials [33]. The experimental set-up is as illustrated in Figure 2-4 [34], where the sample is held in a container within a convection oven. The temperature of the oven is kept at a certain value, while the temperature at the center of the sample is continuously monitored. The procedure is repeated using different oven temperatures and sample container sizes, until the "critical" point – the oven temperature and the sample container size at which the sample becomes unstable – is determined.

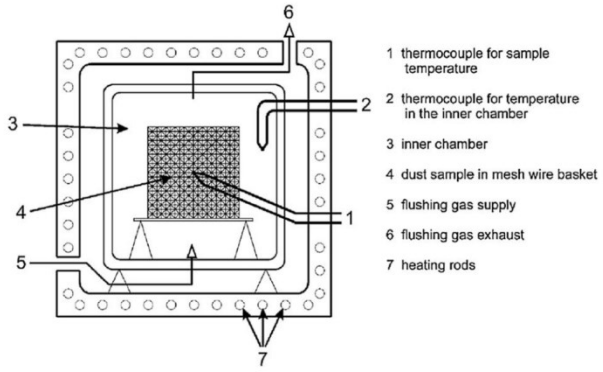

Figure 2-4: Hot Storage Test Set-up

2.1.3.2 Simplified Hot-storage Method recommended by United Nations (UN)

The UN test uses the Hot-Storage method as the standard test methodology to evaluate materials considered as potentially "spontaneously combustible".

According to the UN's "recommendation on transport of dangerous goods" [33], these materials are to be tested before transportation and are to be categorized into groups requiring different transport arrangements.

Procedures recommended by the UN are simpler than the original Hot-Storage test. Instead of running a series of tests to determine the critical value (the oven temperature and the sample container size), the materials are only required to be tested at the given conditions: oven temperatures of 100 °C, 120 °C and 140 °C and sample container sizes of 25 mm and 100 mm. If the sample temperature increases more than 60 °C above the oven temperature within the 24 hours of testing, it is considered "dangerous heating". The order of the tests are specified in the "classification scheme" [35] as illustrated in Figure 2-5.

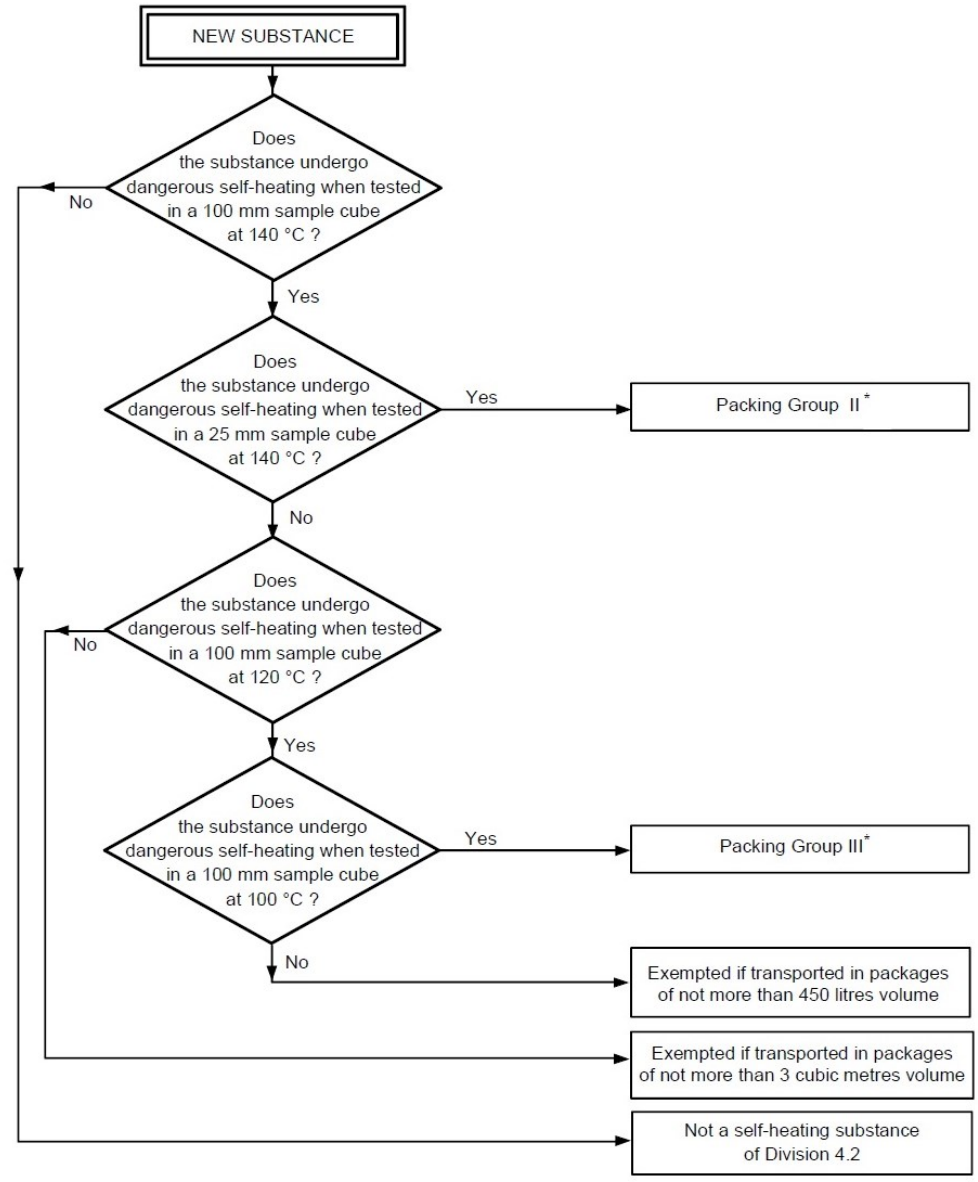

* *Substances with a temperature for spontaneous combustion higher than 50 °C for 27 m^3 should not be classified in Division 4.2.*

Figure 2-5: Classification of Self-heating Substances

2.1.4 Crossing-Point-Temperature (CPT) Method

The CPT method, first developed by Chen and Chong [36], was originally used to investigate the self-heating behaviour of wood particles and milk powders [37]; later this method was found to be effective in testing other materials as well, such as sulphides [29-31], [25]

The experimental set-up is as shown in Figure 2-6 [14]. The sample is placed into a wire mesh basket and put into the convection oven where the temperature is increased to 160 °C and held constant. The temperatures at two locations in the sample are continuously monitored: one at the core (referred to as the core temperature) and one 10 mm away from the center (referred to as the outer temperature).

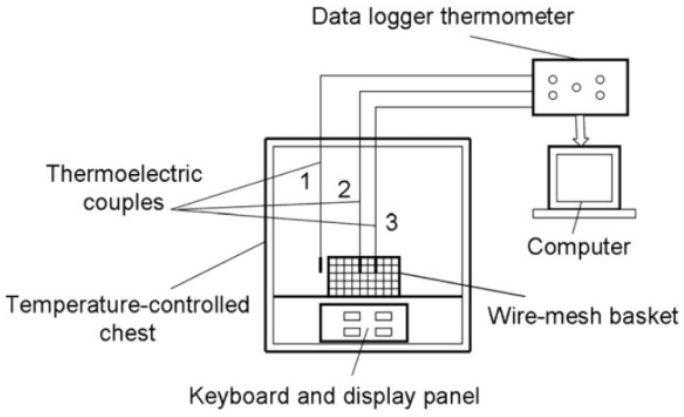

Figure 2-6: CPT Set-up

As shown in Figure 2-7 [14], as the oven temperature rises, both the outer and core sample temperatures increase. Initially, the outer temperature (T_2 in Figure

2-7) is greater than the core temperature (T_1 in Figure 2-7) due to the heat flow into the sample. If the material self-heats, however, the core temperature surpasses the outer temperature, due to the outward heat flux. The point at which T_1 equals T_2 is defined as the "crossing-point temperature", a characteristic property of self-heating materials [36].

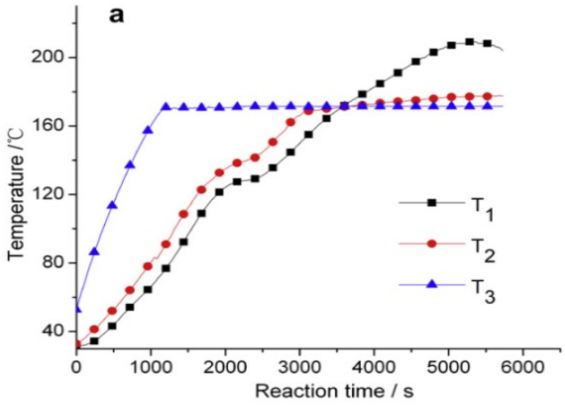

Figure 2-7: CPT Self-heating Curves

2.1.5 Standard Self-heating Test Apparatus

2.1.5.1 Temperature-rise Apparatus

A temperature-rise apparatus, developed by Rosenblum and Spira [38], measures the self-heating rate and the oxygen consumption of sulphides at ambient conditions (stage A). A cross-section of the experimental set-up is as shown in Figure 2-8 [38], where the sample-holding beaker is covered in several layers: a Dewar insulator flask, a Styrofoam container and a copper shield. The copper

shield is wrapped with heating coils in order to maintain the apparatus at a constant temperature of 40 ± 0.2 °C.

A 1-kg sample is moistened and preheated to 28 °C prior to testing, and introduced into the apparatus. The apparatus temperature is held at 40 °C, which gradually brings the sample temperature up to equilibrium at 38.5 °C. An inert material stays at this equilibrium temperature, whereas for a self-heating material the temperature increases above this point. The self-heating rates and the oxygen consumption are measured as the samples self-heat.

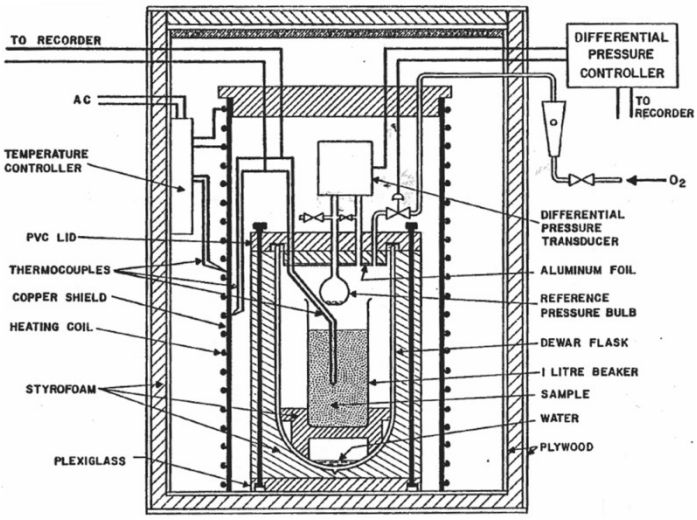

Figure 2-8: Temperature-Rise Apparatus

Table 2-1 is a hazard rating chart [38] constructed by Rosenblum and Spira, after testing some known hazardous materials. This chart can be used as a reference for determining the hazard levels of unknown sulphides.

Table 2-1: Hazard Rating Guide

Self-heating rate, °C/hr	Ore	Hazard Rating
> 3	Horne, Poirier	Hazardous
1	Brunswick	Possibly Hazardous
< 0.5	Geco, Matagami Division	Safe

2.1.5.2 Standard Self-heating Apparatus

An improved version of the temperature-rise apparatus, the "standard self-heating apparatus", was developed by Rosenblum and Spira (Figure 2-9 [39]). Similar to the temperature-rise apparatus, a sample is moistened prior to testing, and introduced into the apparatus. The sample is first tested at stage A condition, where the temperature of the apparatus is set to 70°C, and then tested at stage B condition, where the temperature is set to 140°C. For each stage, air is injected through the sample 10 times, each air injection comprising 15 minutes of air flow at a set rate (100mL/min at Stage A and 250mL/min at Stage B) into the sample, followed by no air flow for 5 hours.

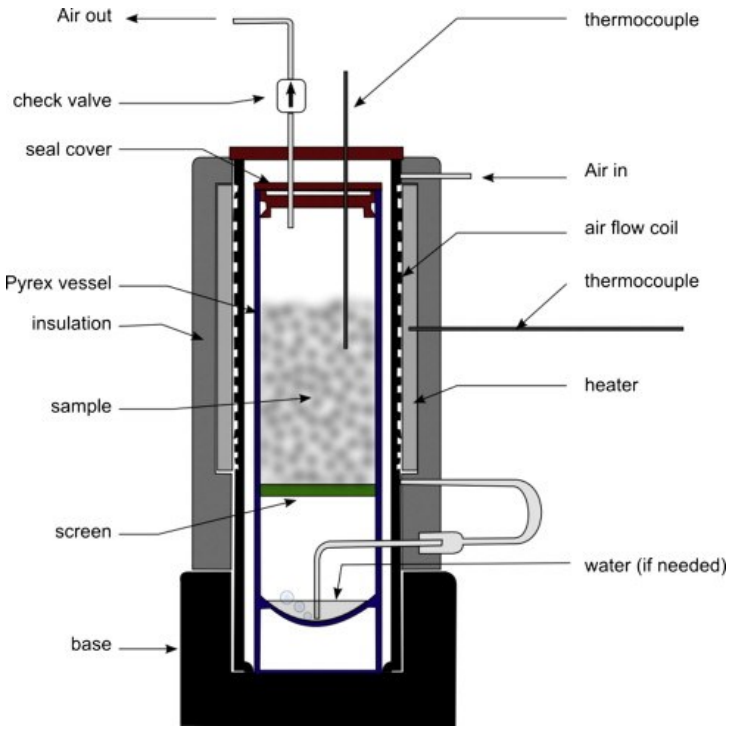

Figure 2-9: Standard Self-heating Apparatus

A complete thermogram of a typical standard test is shown in Figure 2-10 [15], where the primary y-axis indicates the sample temperature in °C and the secondary y-axis indicates the air flow in mL/min. An active sample self-heats during the 15-min of air injection, returning to equilibrium over the five 5-hr interval between air injections.

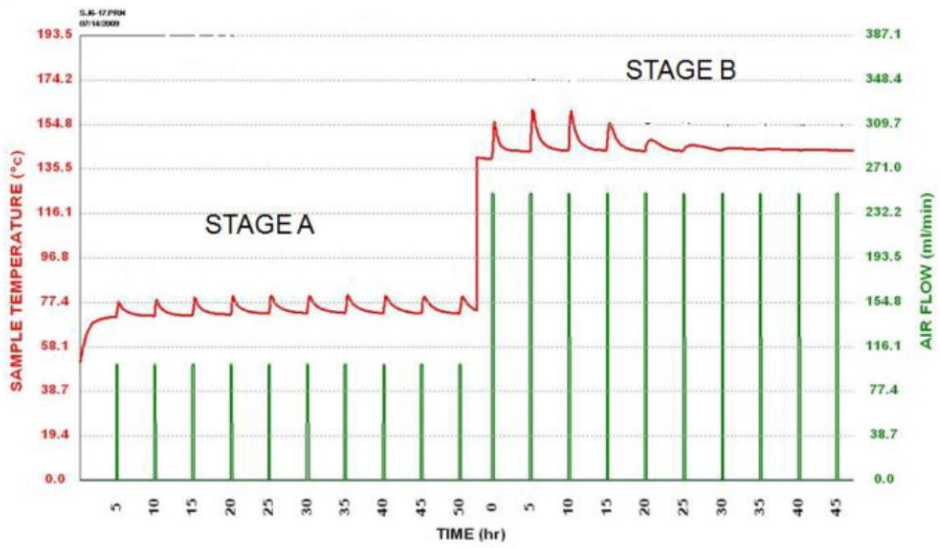

Figure 2-10: Self-heating Thermogram of an Active Sample

2.1.5.3 Weathering Apparatus

A weathering apparatus is used as an alternative to a stage A to give a variety of conditions [24]. This apparatus "weathers" the sample prior to stage B testing; differently weathered samples show different self-heating in stage B.

The first design of a weathering apparatus is as shown in Figure 2-11. Oxygen exposure of the sample is controlled by the number of holes on the cover of the reaction chamber, while the chamber is maintained at a constant temperature of 40 °C.

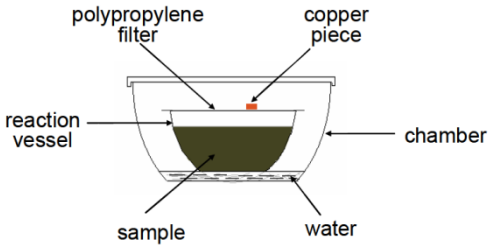

Figure 2-11: Schematic Picture of "Weathering" Apparatus

An improved version of the apparatus is as shown in Figure 2-12 [21]. The improvements allow for monitoring and controlling relative humidity, air temperature and oxygen content within the system.

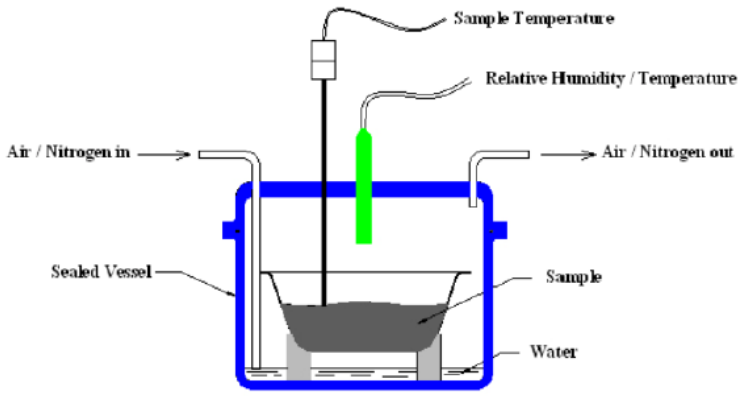

Figure 2-12: Improved Weathering Apparatus

2.1.6 Stockpile Temperature Measurement

Direct stockpile temperature measurement was conducted by Ozdenis and Kelebek [40], from sulphides exposed to atmospheric conditions. Temperatures at 6 different positions of stockpile, (see Figure 2-13 [40]), were recorded each hour

for a total of 4850 hrs and were compared to atmospheric temperature, as shown in Figure 2-14 [40].

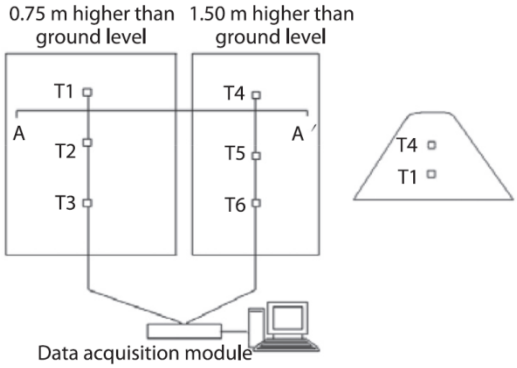

Figure 2-13: Stockpile Measurement

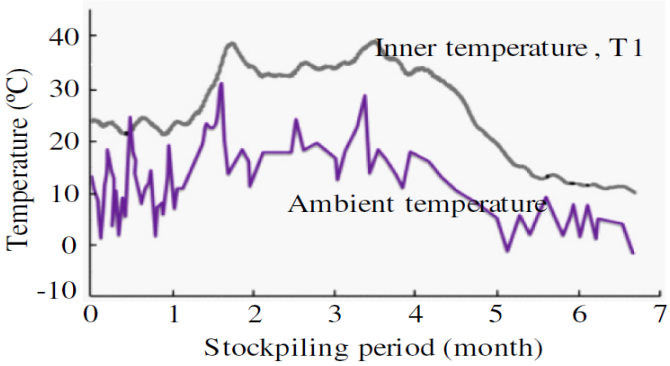

Figure 2-14: Ambient and Stockpile Temperature (T1) as a Function of Time

2.2 Causes and Mitigation

Many factors have shown to affect the self-heating of sulphides. Moisture and oxygen are the most crucial, but temperature, pH, particle size and mineralogical composition also contribute to self-heating reactions. In some cases, it was possible to reduce or delay self-heating by controlling these factors.

2.2.1 Moisture and Oxygen

Moisture and oxygen are required for initial self-heating reactions to take place at ambient temperatures [5, 9, 13, 22, 27]. Rosenblum *et al* [38] showed that a certain range of moisture content is required to promote self-heating of sulphides; no heating at both moisture extremes, namely at 0 % and over 26 % by mass, was observed. Too much moisture can act as a heat sink to prevent self-heating [5], and "water flooding" is sometimes used as a mitigation method [5]. Removal of moisture by adding hygroscopic materials (such as acrylic acid sodium salt [15] and Bentonite mixes [4]) is also suggested as a mitigation method.

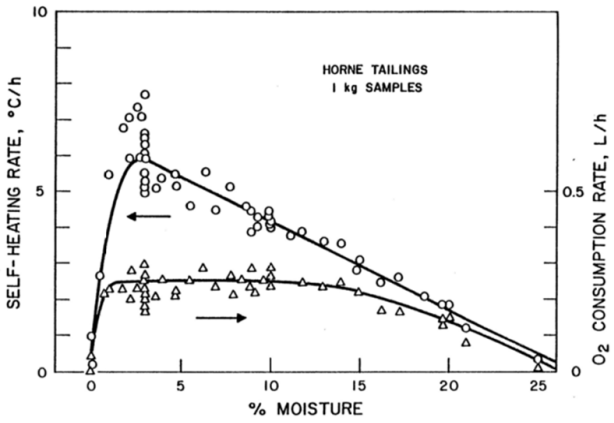

Figure 2-15: Effect of Moisture and Oxygen Consumption on the Self-heating Rate

Dependence of stage A self-heating rates on the amount of oxygen uptake was observed by Rosenblum [13], as shown in Figure 2-16. The role of oxygen in stage B self-heating was observed by Illiyas [30], as shown in Figure 2-17; DSC testing using active sulphide samples showed that the self-heating is only apparent in the presence of oxygen.

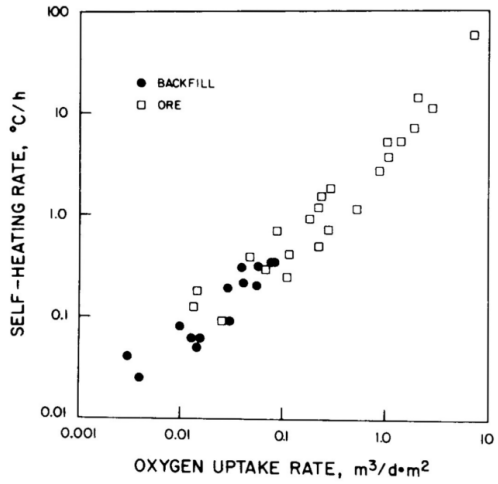

Figure 2-16: Self-heating Rate as a Function of Oxygen Uptake Rate

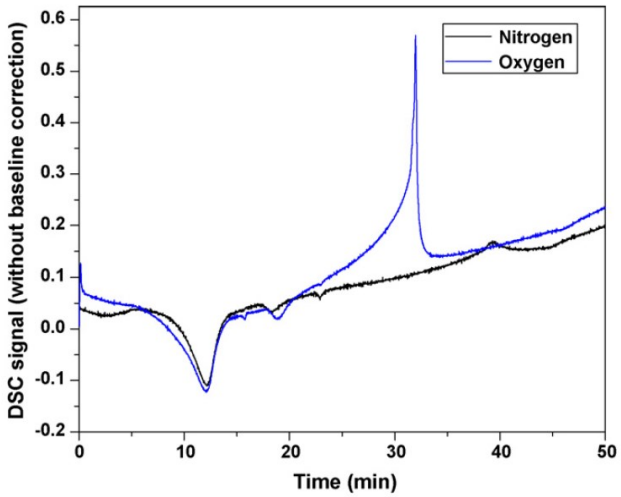

Figure 2-17: DSC Curves

Self-heating can be reduced by blocking the oxygen flow to active sulphides, through surface coverage [9, 16, 17] or mineral coating [19]. A chalcopyrite concentrate stockpile at temperatures of 40 °C to 70 °C was found to cool down to 6 °C to 12 °C, after the installation of a plastic sheet cover for five days [17]. Chemical coating using Alconox and Marasperse were also tested to significantly reduce self-heating of sulphide ores and tailings [9]. Spraying polyethylene polyamine solutions on stockpile surfaces has also been suggested to prevent oxidation of sulphides [19].

2.2.2 Temperature

Elevated temperatures facilitate oxygen diffusion [23] to the sulphide surfaces, and thus influence the level of self-heating. Tests showed that, at elevated temperatures, higher self-heating rates are produced [9] and thus the suppression of self-heating is harder to achieve [9]. Cooling the sulphide system is therefore

suggested as one of the mitigation method; for relatively low-hazard materials, this can be achieved by increasing ventilation in underground mines [17].

2.2.3 pH level and Fe^{3+}

When moisture is provided, sulphides oxidize to produce acid and Fe^{3+}. As the pH level of the system decreases below 4, Fe^{3+} becomes the main oxidizing agent [16, 25]; dependence of pyrrhotite oxidation on Fe^{3+} at this condition is as shown in Figure 2-18 [25].

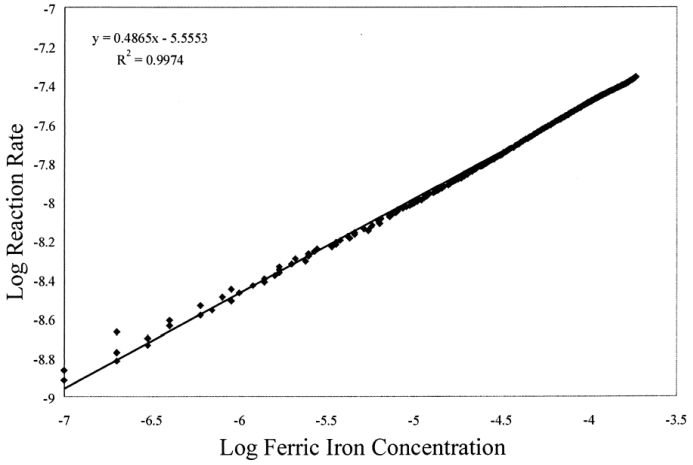

Figure 2-18: The Dependence of Pyrrhotite Oxidation on Fe^{3+}

Suppressing the oxidation by reducing the Fe^{3+} has been suggested as a mitigation method [16, 18]. This can be done by making the moisture of the system less acidic (alkaline [16, 18]), through lime [4, 5] or other base addition. It was also mentioned, however, that neutralization of the moisture may drive the oxidation further, by supporting the forward reaction [5] (Le Chatlier's principle). The

efficacy of these suggested mitigation methods should therefore be further investigated [16].

2.2.4 Pyrrhotite Content

It is well known that pyrrhotite is the most reactive species among the sulfides [5]. Due to its lower activation energy [25], it oxidizes more readily and is more significantly involved in self-heating reactions [14, 29-31]. High content of pyrrhotite (more than 10% by mass) makes samples more prone to self-heating [9, 10]. The oxidation and self-heating reactions of pyrrhotite are discussed in detail in section 2.3.

2.2.5 Elemental Sulfur

The contribution of elemental sulfur on self-heating of sulphides has been extensively studied. Good [4] presumed that the mine fires he experienced are triggered by sensitive areas of sulphides having low ignition points, which included the regions with high elemental sulphur content. As shown in Figure 2-19, his series of combustion tests showed that sulphide ignition temperatures are linked with the elemental content added in the sulphide samples.

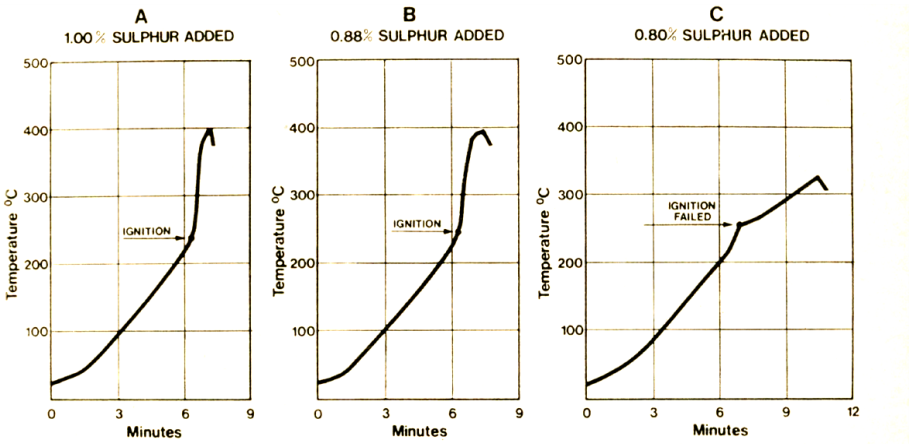

Figure 2-19: Critical Sulfur Determination

Rosenblum[9] also refers to the naturally formed elemental sulfur as "fuel" that contributes to "thermal decomposition" at higher temperatures [4]. Elemental sulfur formation during stage A and its consumption during stage B are as shown in Figure 2-20 [9]. The correlation between the amount of elemental sulfur and self-heating in high temperatures (stages B and C) was also observed by Bouffard [8], using the modified Hot-storage method.

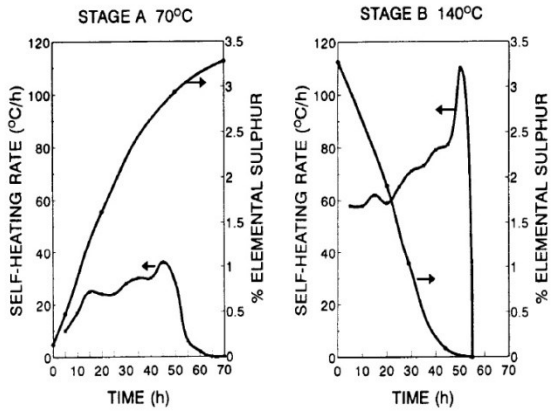

Figure 2-20: Self-heating Rate and Elemental Sulphur Content During Stages A and B

2.2.6 Particle Size

Higher self-heating rates are often associated with sulphides of finer particle size [4]. As shown in Figure 2-21, for active sulphides fine grinding increased the self-heating rates. Some inactive sulphides were observed to become active when reduced in particle size [41]. Ground sulphides are therefore listed as the materials of potential self-heating hazard [38], and smaller blasts in mining are suggested to minimize formation of fine particles[4, 9].

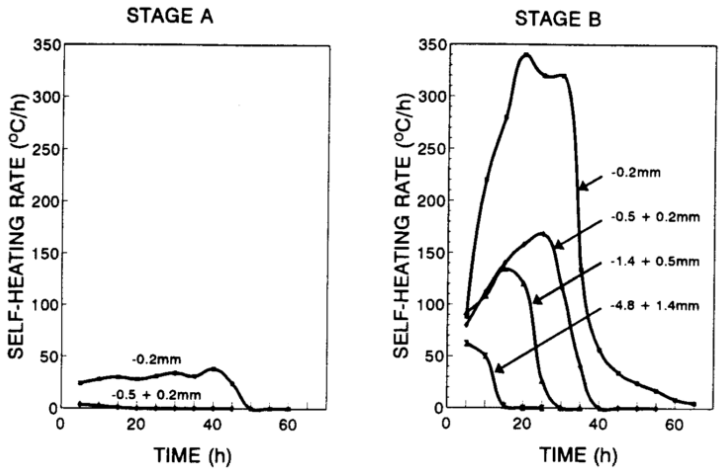

Figure 2-21: Effect of Particle Size on Self-heating Rate in Stages A and B

2.2.7 Galvanic Interaction

Galvanic interactions describe the electrochemical reaction between various mineral phases in contact that have different rest potentials [42, 43]; this may affect self-heating by modifying the reaction rates of sulphides [42-44]. Most times, sulphide samples are mixtures of sulphides, naturally forming galvanic cells [43]. A sulphide with higher rest potential is called the cathode and the lower

rest potential, anode. The anodic and cathodic half-cell reactions proceed through equations (4.1) and (4.2), respectively.

$$MeS \rightarrow Me^{2+} + S^0 + 2e^- \quad (4.1)$$

$$0.5\ O_2 + 2\ H^+ + 2\ e^- \rightarrow H_2O \quad (4.2)\ a$$

$$Fe^{3+} + e^- \rightarrow Fe^{2+} \quad (4.2)\ b$$

Sulphide mixtures of different rest potentials have been tested by Payant [41] using the standard self-heating apparatus. Greater self-heating was observed for mixtures involving a higher rest potential difference. Pyrite, acting as the anode, in the mix was particularly active in promoting self-heating. Mitigation measures to overcome this effect include: 1) decreasing the pyrite content to below 10 % [18], and 2) placing electrodes in the sample and applying an electrical potential to counter the effect [16].

2.3 Oxidation Reactions and Self-heating

An agreed self-heating mechanism has not been clearly identified to date [4]. A complex matrix of oxidation reactions exists under ambient conditions, which may directly or indirectly contribute to self-heating. Ongoing investigations of reaction mechanisms aim to develop proper mitigation controls in the future [11].

Possible sulphide oxidation reactions are reviewed in this section. Since pyrrhotite is mostly prone to self-heating compared to other sulphides [9, 11], its oxidation reactions are reviewed in detail. Direct oxidation of pyrrhotite are referred to as

"primary oxidation" and oxidation of intermediate products are referred to as "secondary oxidation"; it is possible for primary and secondary reactions to occur simultaneously.

2.3.1 Primary Reactions

2.3.1.1 Condition: Oxygen and Moisture

In the presence of moisture and oxygen, it is believed that pyrrhotite self-heats through equations (1) to (4), producing elemental sulfur (S), goethite (FeO.OH), and iron sulphate [5, 18, 22]. These products were observed to form after a self-heating test conducted at 50°C with 6% moisture by mass [9], and also after an oxidation test conducted at 52°C with 68% relative humidity [18]. It was noted that more FeO·OH and S were formed than iron sulphate.

$$FeS + 2\ O_2 + 7\ H_2O \rightarrow FeSO_4{\cdot}7H_2O \quad (1)$$

$$2\ FeS + 4\ O_2 + 8\ H_2O \rightarrow FeSO_4{\cdot}H2O + FeSO_4{\cdot}7H_2O \quad (2)$$

$$4FeS + 3O_2 + 2H_2O \rightarrow 4FeO{\cdot}OH + 4S \quad (3)$$

$$2\ Fe_7S_8 + 10.5\ O_2 + 7\ H_2O \rightarrow 14\ FeO(OH) + 16\ S° \quad (4)$$

Acidification can also take place [22, 25] through equations (5) and (6); it was observed that the system becomes acidic after the sulphides were oxidized in stage A conditions [9]. The acid-generating reactions are not specifically known

as self-heating reactions; however, some major self-heating reactions may depend on this step.

$$Fe_{1-x}S + (2 - 0.5x)\ O_2 + xH_2O \rightarrow (1 - x)\ Fe^{+2} + SO_4^{-2} + 2x\ H^+ \qquad (5)$$

$$2\ Fe_7S_8 + 31\ O_2 + 2\ H_2O \rightarrow 14\ FeSO_4 + 2\ H_2SO_4 \qquad (6)$$

Oxides are also formed through equation (7) [4]. Oxide formation is known to release free energy ranging from 85 to 170 kJ/mol [16], and is involved in further secondary self-heating reactions.

$$4\ FeS + 7\ O_2 \rightarrow 2\ Fe_2O_3 + 4\ SO_2 \qquad (7)$$

2.3.1.2 Condition: Oxygen, Moisture and Low pH

Once acidified, more reaction routes are available for pyrrhotite. Equations (8) and (9) describe the formation of Fe^{2+}, as well as H_2S [4, 16, 25, 27]. Both of these reactions influence the self-heating; H_2S later proceeds to further self-heating reactions and Fe^{2+} later generates Fe^{3+}, a main oxidizing agent at pH levels lower than 4 [25, 27].

$$Fe_{1-x}S + 2\ (H^+)_{aq} \leftrightarrow (1 - x)\ (Fe^{+2})_{aq} + (H_2S)_g \qquad (8)$$

$$FeS + H_2SO_4 \rightarrow FeSO_4 + H_2S \qquad (9)$$

Most oxidation reactions are carried out by ferric Fe^{3+} at this condition (low pH); however, pyrrhotite can still be oxidized by oxygen through partial oxidation, as shown in equation (10), forming Fe^{2+} and elemental sulfur [25].

$$Fe_{1-x}S + ((1-x)/2)\ O_2 + 2(1-x)\ H^+ \leftrightarrow (1-x)\ Fe^{+2} + (1-x)\ H_2O + S° \quad (10)$$

2.3.1.3 Condition: Oxygen, Moisture, Low pH and Fe3+

Acidic conditions allow for the formation of Fe^{3+}, which acts as a main oxidizing agent at low pH. Pyrrhotite oxidation through these species generates Fe^{2+}, sulfates, elemental sulfur and more acid, as shown in equations (11) and (12) [16, 25, 27].

$$Fe_{1-x}S_{(s)} + (8-2x)\ Fe^{+3} + 4\ H_2O \rightarrow (9-3x)\ Fe^{+2} + SO_4^{-2} + 8\ H^+ \quad (11)$$

$$Fe_{1-x}S_{(s)} + (2-2x)\ Fe^{+3} \rightarrow (3-3x)\ Fe^{+2} + S°_{(s)} \quad (12)$$

Partial oxidation reactions through Fe^{3+} are as shown in reaction (13) and (14); Fe^{+2} and sulfur-rich pyrrhotite [25] may be produced through reaction (13), or goethite, elemental sulfur and more acid [45] through reaction (14).

$$Fe_{1-x}S + 2y\ Fe^{+3} \rightarrow 3y\ Fe^{+2} + Fe_{1-x-y}S \quad (13)$$

$$Fe_{1-x}S_{(s)} + Fe^{+3}{}_{(aq)} + ¾\ O_2 + 5/2\ H_2O \rightarrow 2FeO{\cdot}OH + S° + 3\ H^+ \quad (14)$$

2.3.2 Secondary Reactions

2.3.2.1 Condition: Oxygen and Moisture

In neutral or mildly acidic conditions, ferric ions often precipitate as oxides and produce acid through reactions (15) and (16) [4, 25, 45].

$$Fe_2(SO_4)_3 + 6\ H_2O \rightarrow 2\ Fe(OH)_3 + 3\ H_2SO_4 \quad (15)$$

$$Fe^{2+} + ¼\ O_2 + 5/2\ H_2O \rightarrow Fe(OH)_{3(s)} + 2\ H^+ \quad (16)$$

H_2S formed through primary oxidation may oxidize further through highly exothermic reactions. Possible oxidation routes have been suggested by Somot [4, 10] and Good [4, 10] as shown in equations (17) to (21). The significance of H_2S oxidation on stage A of self-heating was proved by Somot [10, 11]; immediate removal of H_2S, thus blocking the H_2S oxidation, decreased the self-heating rates of sulphides.

$$H_2S_{(g)} + ½\ O_2 \rightarrow S° + H_2O \qquad \Delta H = -260\ kJ/mol \quad (17)$$

$$H_2S_{(g)} + O_2 \rightarrow ¼\ S_8° + H_2O_{(aq)} \quad (18)$$

$$H_2S_{(g)} + ½\ O_2 \rightarrow SO_{(g)} + H_2O_{(aq)} \quad (19)$$

$$H_2S_{(g)} + 1½\ O_{2(g)} \rightarrow SO_{2(g)} + H_2O_{(aq)} \qquad \Delta H = -560\ kJ/mol \quad (20)$$

$$H_2S_{(g)} + 2\ O_{2(g)} \rightarrow 2\ H_2SO_{4(aq)} \qquad \Delta H = -870\ kJ/mol \quad (21)$$

Naturally formed elemental sulfur is often suspected of producing self-heating in further reactions [4, 9, 46], through production of sulfates or sulfur dioxide [9, 45], as shown in equations (22) and (23). Formation of SO_2 is suggested to be a significant source of heating within stage B [9].

$$S° + O_2 \rightarrow SO_2 \quad (22)$$

$$S° + 1\ 1/2\ \ O_{2(aq)} + H_2O_{(l)} \rightarrow 2\ H^+_{(aq)} + SO_4^{2-}{}_{(aq)} \quad (23)$$

Other possible reactions include (24) and (25). Once SO_2 is formed, it reacts further with H_2O to produce sulfite species which may be involved in other reactions that contribute to self-heating [4]. Oxidation of Fe^{2+} sulfate to Fe^{3+} sulfate, coupled with $Fe(OH)_3$ precipitation has also been suggested by Wu [22].

$$SO_2 + H_2O \rightarrow H_2SO_3 \quad (24)$$

$$12\ FeSO_4 + 6\ H_2O + 3\ O_2 \rightarrow 4\ Fe_2(SO_4)_3 + 4\ Fe(OH)_3 \quad (25)$$

2.3.2.2 Condition: Oxygen, Moisture and Low pH

Within acidic conditions, ferrous Fe^{2+} oxidizes to produce ferric Fe^{3+} through equation (26), which becomes the oxidizing agent in acidic conditions [25, 27]. Other reactions of Fe^{2+} include the formation of Fe^{3+} sulfate[4, 22], as shown in equation (27). Iron oxides react with acid to form elemental sulfur, Fe^{3+} sulfate and iron sulfite, as shown in equations (28-30) [4].

$$2\ Fe^{2+} + ½\ O_2 + 2\ H^+ \rightarrow 2\ Fe^{3+} + H_2O \quad (26)$$

$$2\ FeSO_4 + ½\ O_2 + H_2SO_4 \rightarrow Fe_2(SO_4)_3 + H_2O \quad (27)$$

$$Fe_2O_3 + 3\ H_2SO_4 \rightarrow Fe_2(SO_4)_3 + 3\ H_2O \quad (28)$$

$$Fe_2O_3 + 4\ H_2SO_3 \rightarrow 2\ FeSO_4 + S° + H_2SO_4 + 3\ H_2O \quad (29)$$

$$Fe_2O_3 + 9\ H_2SO_3 \rightarrow 2\ FeSO_3 + 2\ S° + 5\ H_2SO_4 + 4\ H_2O \quad (30)$$

2.3.2.3 Condition: Oxygen, Moisture, Low pH and Fe^{3+}

Ferric ions may hydroyze to precipitate as oxy-hydroxides. Since acids are products of these reactions, highly acidic conditions will favour the reverse reaction [25].

$$Fe^{3+} + 3\ H_2O \rightarrow Fe(OH)_{3(s)} + 3\ H^+ \quad (31)$$

$$Fe^{3+}_{(aq)} + 2\ H_2O_{(l)} \rightarrow \alpha\text{-}FeO{\cdot}OH_{(s)} + 3\ H^+_{(aq)} \quad (32)$$

3 Experimental Work

3.1 Materials and Sample Preparation

3.1.1 Mill and Mine Site Samples

Samples of Glencore Xstrata's Strathcona mill tailings (Sudbury) were shipped wet and were prepared as described by Payant [47] for drying and homogenization. The dry samples were divided into 500g portions, individually packed into plastic bags and stored in a freezer to prevent oxidation. The main components of the sample were identified by X-ray Diffraction (XRD, described in Section 3.4.2) to be: pyrrhotite, magnetite and silicates. The particle size was 80% passing 38μm.

Samples of mine site ores were shipped from Vale's Voisey's Bay Mine and prepared in similar fashion. Dried samples were divided into 500g portions in a plastic bag and stored in a freezer. The main components of the sample, identified by XRD, were: pyrrhotite, pentlandite, hematite, and silica. The particle size was 80% passing 130μm.

3.1.2 Single Mineral Specimens and Mixtures

Pyrite and pyrrhotite specimens were purchased from Ward's Science. Pyrite samples were ground to 80% passing size 75μm, while pyrrhotite samples were ground to 80% passing size 108μm. Silica sand with 80% passing size 180μm was obtained from the laboratory stock. Three artificial mixtures were made using the

three specimens: 20% pyrrhotite with 80% sand, 20% pyrrhotite with 80% pyrite, and 100% pyrite, by mass.

3.2 Self-heating Measurement

3.2.1 Selection of Measurement Technique

All self-heating tests were conducted using the self-heating apparatus developed by Rosenblum and Spira [17]. Among the various methods introduced in Section 2.1, this particular method was chosen because it measures the self-heating in both stages A and B, while most other techniques measure the self-heating associated with a single stage (A, B, or C). As mentioned in Section 1.1.2.2, sample weathering affects results in both stage A and stage B of the self-heating test. The apparatus therefore meets the present requirement of investigating the relationship between weathering and stage B self-heating.

3.2.2 Self-heating Apparatus

The apparatus is shown in Figure 3-1 [9]. The sample is housed in a 2L Pyrex vessel located inside a temperature-controlled oven. The oven temperature is set at a pre-selected value and the system is allowed to heat up to equilibrium. Once equilibrium is reached, air is introduced through the base of the Pyrex container and flows up through the sample.

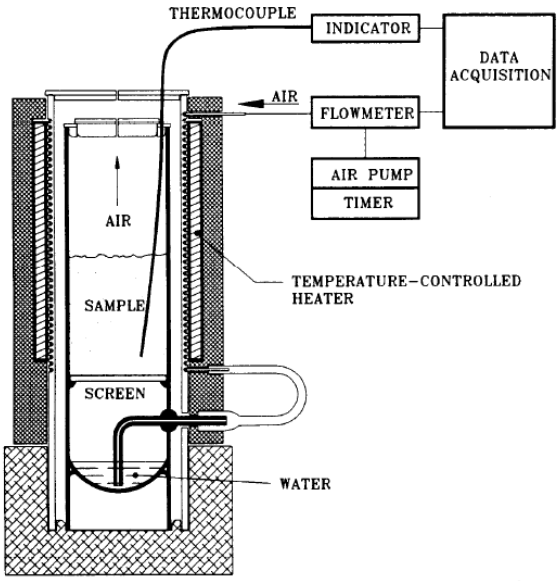

Figure 3-1: Self-heating Measurement Apparatus

Air is introduced for 15 minutes every 5 hours; this 5-hour period is referred to as one "air injection cycle". A thermocouple located at the midpoint of the sample records the sample temperature during the test. An active sample will exhibit a temperature rise during air injection while there will be no noticeable temperature rise for an inactive sample. Some samples exhibit no self-heating for the first few air injection cycles then become active, as mentioned in Section 1.1.3.1.

3.2.3 Standard Self-heating Test

In a standard self-heating test, 500g of the dry sample is first moisturized to 6% moisture. The sample is then tested at two consecutive stages, namely stage A and stage B.

Stage A Procedure:

In stage A, the oven temperature is set to 70°C. Flow rate during each air injection cycle is set to 100mL/min, for a total of 10 injection cycles. Following the 10 cycles, the oven is turned off to cool down to room temperature, and 20g of core sample are collected for sample characterization (e.g., sulfur content) using a thin-walled sampling tube; the test then continues to the stage B procedure.

Stage B Procedure:

In stage B, the oven temperature is set to 140°C. During the initial heat-up period, a continuous flow of nitrogen gas is used to drive off the moisture and ensure a non-oxidizing environment. Once the temperature reaches equilibrium, the sample is then subjected to the same 15 minute air injection every five hours as in stage A but at an air flow rate of 250mL/min for each injection cycle. The test continues (i.e., the air injection schedule is maintained) as long as there is measurable temperature rise during the air injection. The test is stopped when there is no further observable self-heating. Once the oven cools down to room temperature, 20g of sample are again collected for characterization.

3.2.4 Output of Self-heating Test

Figure 3-2 shows a typical thermogram of an active sample tested under standard test conditions. The vertical lines represent the air injections, with the corresponding scale shown on the right. The saw-tooth pattern indicates the

temperature rise during air injections, with the corresponding scale shown on the left. The value shown above each temperature rise is the slope, taken as the self-heating rate (SHR), in °C/hr. A self-heating capacity (SHC) is calculated taking the sum of the SHRs, as shown in Equation 3.1. SHC is considered to be a property of a sample [17].

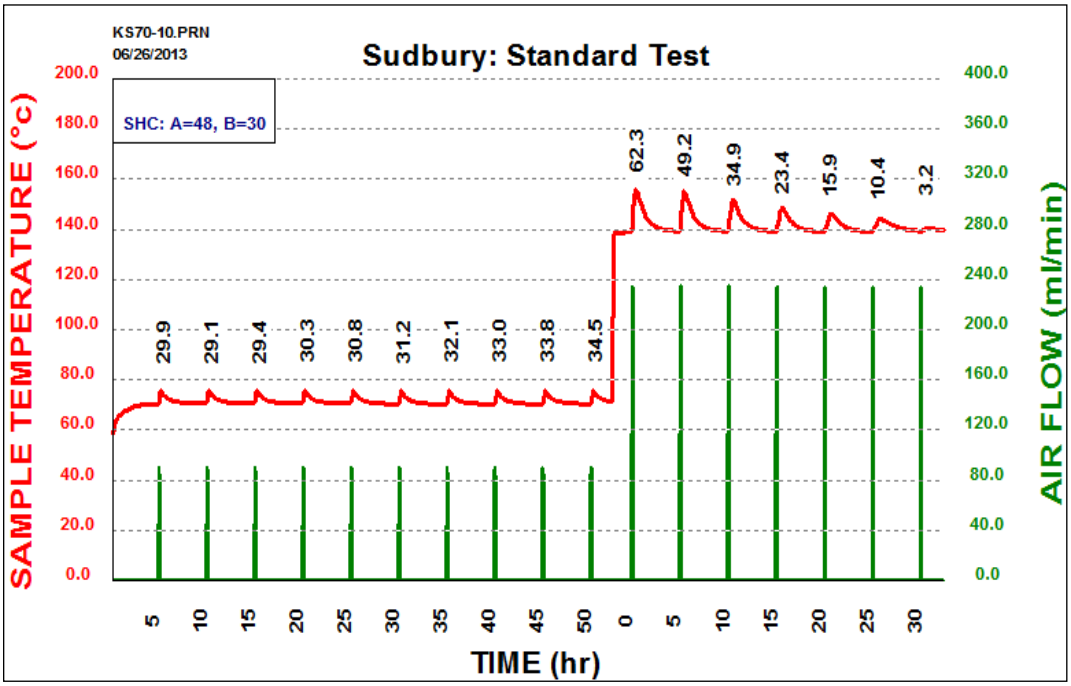

Figure 3-2: Thermogram generated from a standard test

SHC = ∑(SHR of each injection · specific heat of the sample[1]· injection time) (3.1)

= specific heat of the sample · injection time · ∑ (SHR of each injection)

= 0.15 · ∑ (SHR of each injection)

3.3 Experimental Set-up

3.3.1 Weathering Test Procedure

As noted in Section 1.1.2.2, stage A is a weathering stage. To further investigate the effect of weathering, the standard test is modified by varying the stage A temperature and number of air injection cycles, while holding other parameters the same as the standard test conditions.

The two samples described in Section 3.1.1 were tested. The stage A temperatures were set at 40, 55, 60 and 70°C for the Voisey's Bay sample, and at 30, 40, 50, 60 and 70°C for the Sudbury sample. Stage A air injection cycles were set to 10, 20 and 40 for both samples.

The objective was to determine the effect of weathering on formation of elemental sulfur and the resulting self-heating in stage B.

[1] The specific heat of sulfides is estimated at 0.6 J/g

3.3.1.1 Additional tests

Some additional weathering tests were conducted using the same samples. The purpose of these tests was to support the results obtained from the original set of tests.

For the Voisey's Bay sample, the additional tests were: 1) weathering test at 70°C with stage A airflow of 100mL/min for 80 injection cycles, 2) weathering at 70°C with stage A airflow of 300mL/min for 10 and 40 injection cycles. For the Sudbury sample, the additional tests were weathering tests at 70°C with stage A airflow of 300mL/min, for 10, 20 and 40 injection cycles.

3.3.2 Weathering through Induction Period

As mentioned in Section 1.1.3.1, some samples exhibit an induction period before self-heating starts. Both the Voisey's Bay and Sudbury samples exhibited induction period at the lower stage A temperatures. To investigate the effect of weathering during the induction period, sets of tests were conducted with modified stage A temperature and number of injection cycles. Temperature was lowered to 40°C for the Voisey's Bay sample and to 30°C for the Sudbury sample; the number of stage A injection cycles were varied from 0 (direct stage B testing of the sample), 18 and 20 for Voisey's Bay and to 0, 7 and 10 for Sudbury sample. Other parameters stayed the same as the standard test conditions.

The objective of the test was to investigate the effect of induction period on formation of elemental sulfur and the resulting self-heating in stage B.

3.3.3 Recycle Test Procedure

The recycle test procedure consists of a series of standard tests conducted on the same sample. At the end of each test – stage A followed by stage B – the sample is remoistened and retested. The procedure is continued until there is no further heating observed in either stage A or stage B. The total amount of heat generated in each test series is calculated and defined as the heat generating capacity (HGC); this value is a sum of all the SHCs generated during each of the stages, as shown in Equation 3.2. All samples introduced in Section 3.1 were tested using the recycle test procedure.

$$\text{Stage A HGC} = \sum (\text{SHC A}) \qquad (3.2)$$

$$\text{Stage B HGC} = \sum (\text{SHC B})$$

The objectives of this test were: 1) to measure the HGC of the samples, 2) to establish a relationship between elemental sulfur formed during stage A and the subsequent heating in stage B, and 3) to track the composition/mineralogy of the sample as it progressively oxidizes.

3.3.3.1 Additional tests

Additional tests were conducted using both the Voisey'Bay and Sudbury samples by increasing airflow in stage A to 300mL/min. The purpose of these tests was to investigate the effect of stage A airflow (while keeping the other parameters unchanged) on sulfur generation and self-heating in stage B.

3.4 Sample Characterization

3.4.1 Elemental Sulfur Analysis

All samples were analysed for elemental sulfur using the carbon disulfide method, described by Jung [15]. As recommended, the procedure was refined to raise the carbon disulfide from 20 to 25mL per 5g of sulfide sample. Carbon disulfide (99.9%, Sigma-Aldrich A.C.S. reagent grade) was used, and consistent results were produced [15].

3.4.2 X-ray Diffraction

X-ray diffraction was conducted on selected samples using the Bruker D8 Discover. Operating conditions were 35kV and 45mA. Software used for this technique include: GADDS for operation, EVA for merging the frames, and X-Pert-Highscore for phase analysis.

3.4.3 X-ray Photoelectron Spectroscopy (XPS)

XPS measurements were carried out on selected samples using the K-Alpha, Thermo Scientific instrument. A pass energy of 50eV with X-ray spot size of 200um was used; the analytical chamber pressure was on the order of 10^{-7}Pa. A flood gun was used to neutralize surface charge build-up. Operation and analysis of peaks were both done using Avantage software.

3.4.4 Electron Microprobe Analysis

The microprobe analysis was performed by the Earth and Planetary Sciences Department of McGill University, using the JEOL JXA-8900 Electron

Microprobe. The 3 more relevant samples were selected for the analysis. In each of the samples, only the pyrrhotite particles were analysed. Operating conditions were an accelerating voltage of 20kV and beam current of 30nA with a beam size of 3µm. During the spot elemental composition analysis, counting time was held constant at 20s for all selected elements: S, Fe, Ni, Co, Zn and Cu. Sample polishing was done using the Vancouver Petrographics LTD polisher prior to analysis.

3.4.5 Inductively Coupled Plasma - Optical Emission Spectrometry (ICP-OES)

ICP-OES (Trace Scan, Thermo Scientific) analysis was performed on selected samples for bulk iron and sulfur mass composition. Trace scan software was used for data processing. Acid digestion was performed prior to analysis, using 70% Nitric acid and 37% Hydrochloric acid. Standards were made by diluting 1000ppm Iron and Sulfur standards.

4 Results

4.1 Weathering Test

In a standard self-heating test, the sample is first tested at Stage A, where the temperature is set to 70°C and the air flow rate is set to 100mL/min for a total of 10 injection cycles. The stage A-tested sample is then tested at stage B, as described in Section 3.2.3.

In the weathering test procedure, the self-heating tests are conducted with modified stage A conditions (Section 3.3.1), while stage B conditions stay the same as the standard test conditions. The effect of various weathering conditions (Stage A modifications) on (1) self-heating in stage A, (2) formation of elemental sulfur, and (3) the resulting self-heating in stage B are presented in this section.

4.1.1 Self-heating in Stages A and B

4.1.1.1 Self-heating Rate (SHR)

The self-heating rate, SHR (Section 3.2.4), represents the increase in the sample temperature during each air injection cycle; this is determined from the thermogram generated from each self-heating test.

Voisey's Bay Sample

The Voisey's Bay sample was tested at the following stage A conditions: 10, 20 and 40 air injection cycles at 40, 55, 60 and 70°C. The results obtained from the 40-cycle tests (40 air injection cycles at 40, 55, 60 and 70°C) are shown in Figure 4-1, where the SHRs generated at each air injection are plotted against the injection numbers.

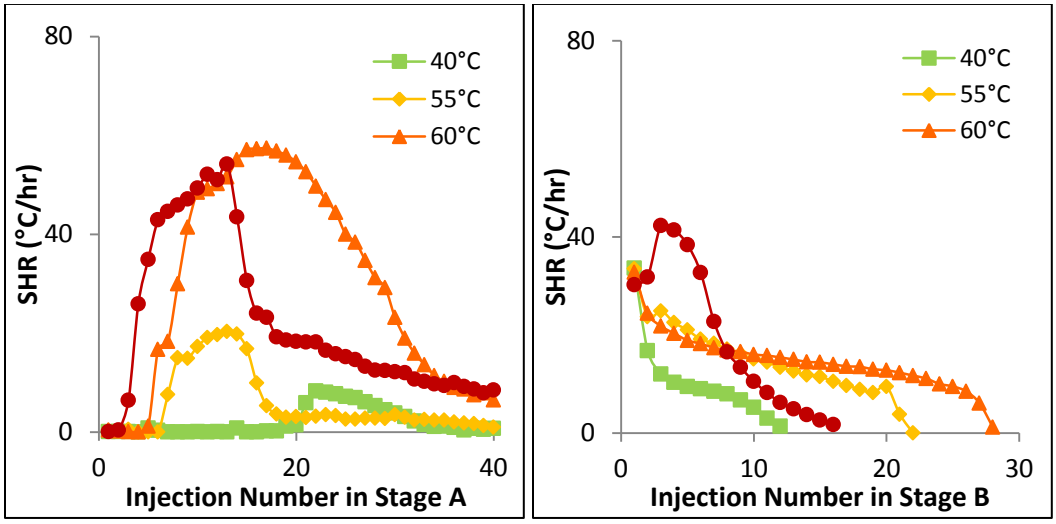

Figure 4-1: SHR Generation of the Voisey's Bay Sample: a) Stage A SHRs and b) Stage B SHRs

During stage A (Figure 4-1-a), no response was observed at the start of the tests, due to the sample exhibiting a delay on the onset of self-heating (Section 1.1.3.1). Upon further air injections, the SHR started to increase, reached a maximum, and then decreased. At 40°C, the sample exhibited practically no self-heating for the first 18 air injections; after this delay, self-heating started from the 19th air injection and lasted until the 35th air injection. The tests conducted at higher

temperatures (55, 60, and 70°C) showed shorter periods of delay, followed by longer periods of self-heating.

It was observed that the self-heating in stage B was contingent on the stage A temperature, as shown in Figure 4-1-b. The highest self-heating rates were generally observed for the first air injection, and gradually decreased upon further air injections. In contrast with other tests, the samples weathered at 70°C showed an increase in the self-heating rate upon the first three air injections and gradually decreased upon further air injections.

Sudbury Sample

The Sudbury sample was tested at the following stage A conditions: 10, 20 and 40 air injection cycles at 30, 40, 50 and 60°C. The results obtained from the 40-cycle tests are shown in Figure 4-2.

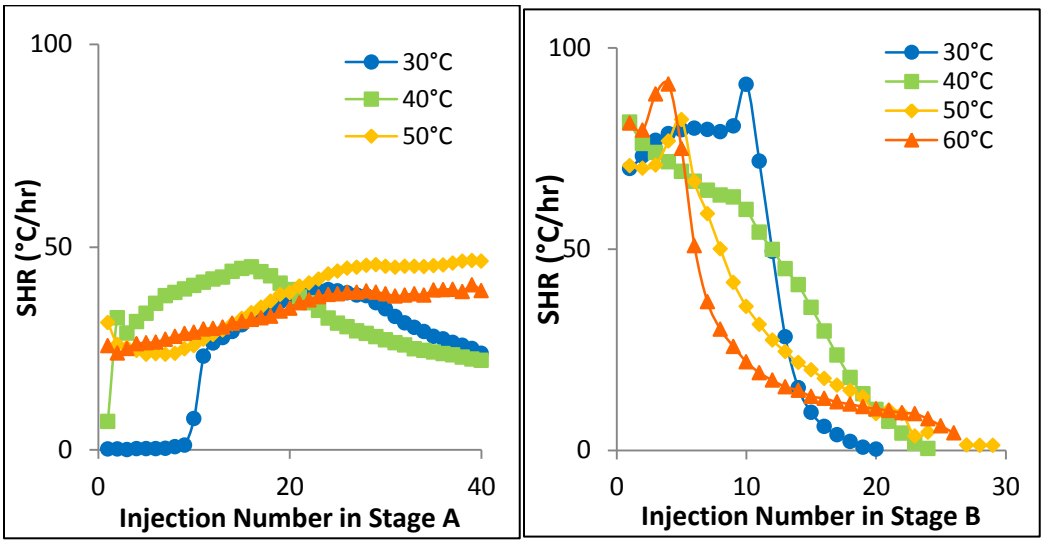

Figure 4-2: SHR Generation of the Sudbury Sample: a) Stage A SHRs and b) Stage B SHRs

With the Sudbury sample, as opposed to the Voisey's Bay sample, the delay in stage A self-heating was only observed at 30°C.

During stage B (Figure 4-2-b), the SHRs generally increased for the first few air injections, followed by a rapid decrease. In contrast with other tests, the 40°C-test produced maximum SHR on the first air injection, followed by a gradual decrease upon further injections.

4.1.1.2 Self-heating Capacity (SHC)

The self-heating capacity, SHC (Section 3.2.4), represents the magnitude of self-heating produced by a particular sample, during a self-heating stage (stage A or stage B). The SHC obtained from the weathering tests was observed to be affected by the number of air injection cycles and the temperatures in stage A.

SHC as a Function of Stage A Temperatures

Figure 4-3 shows the SHC generated by the Voisey's Bay sample, plotted against the stage A temperatures. Both the stage A and the stage B SHC were contingent on the stage A temperatures; the maximum SHC were observed when the sample was tested at stage A temperatures of (1) 60°C for the 20 and 40 cycle tests, and (2) 70°C for the 10 cycle tests.

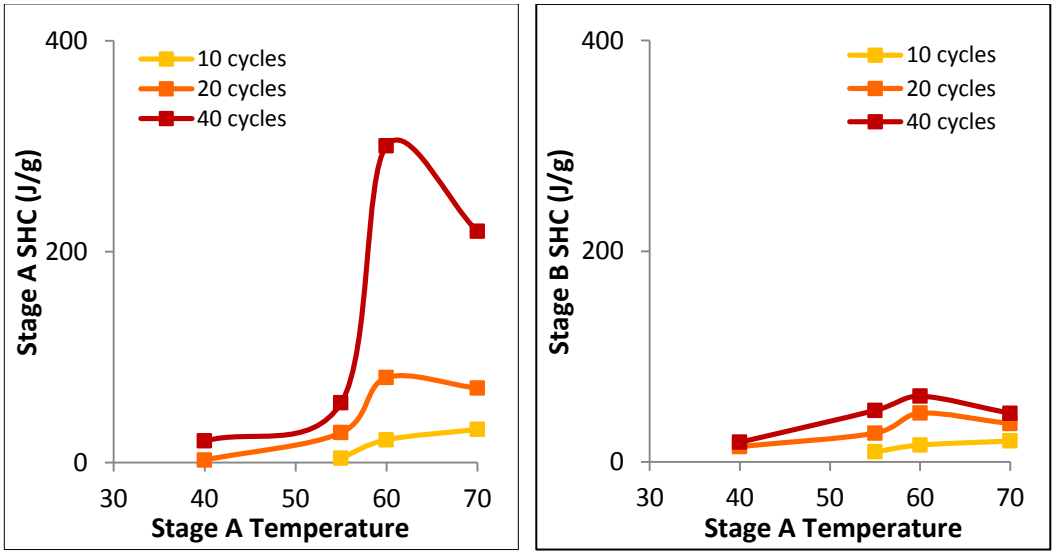

Figure 4-3: SHC as a Function of Stage A Temperatures, Voisey's Bay Sample: a) Stage A SHC and b) Stage B SHC

Figure 4-4 shows SHC generated by the Sudbury sample, plotted against the stage A temperature. Similar to the Voisey's Bay sample, both stage A and stage B SHCs were contingent on the stage A temperatures. The maximum stage A SHC was observed when the sample was tested at stage A temperatures of (1) 40°C for 10 cycle tests, and (2) 50°C for 20 and 40 cycle tests. The maximum stage B SHC

was observed when the sample was tested at stage A temperatures of (1) 40°C for 10 and 40 cycle tests, and (2) 60°C for 20 cycle tests.

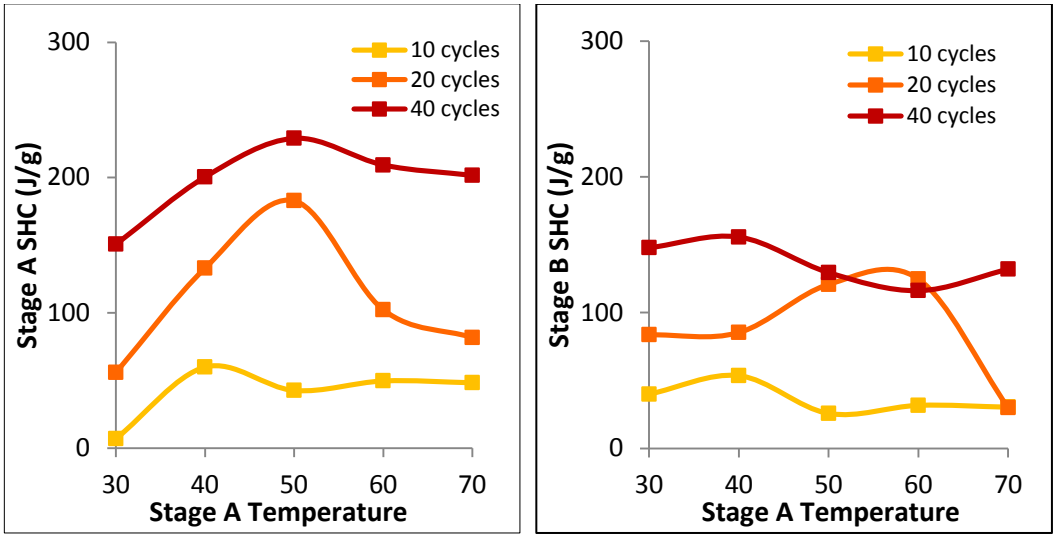

Figure 4-4: SHCs as a Function of Stage A Temperatures, Sudbury Sample: a) Stage A SHCs and b) Stage B SHCs

SHC as a Function of Stage A Air Injections

Figure 4-5 shows SHC generated by the Voisey's Bay sample, plotted against the number of air injections in stage A. Both the stage A and the stage B SHCs were observed to increase with increasing number of air injections in stage A.

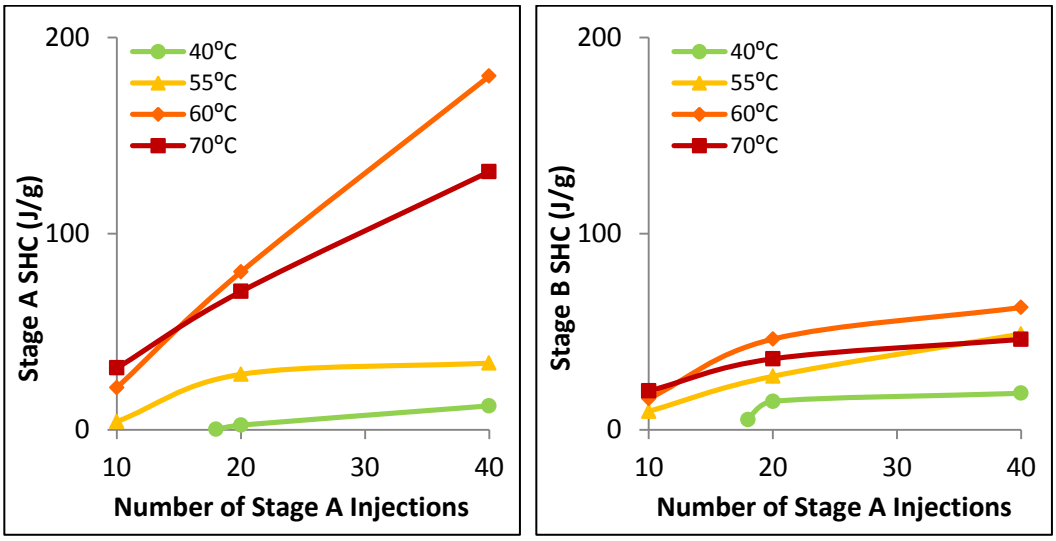

Figure 4-5: SHCs as a Function of Number of Stage A Injections, Voisey's Bay Sample: a) Stage A SHCs and b) Stage B SHCs

To determine whether the increasing trend of the SHC continued, an additional test was conducted at 70°C with additional stage A air injections (80 cycles) and the results were added to the previous data set; Figure 4-6 shows the results obtained from all 70°C-tests (70°C-tested for 5, 10, 20, 40, and 80 cycles). Upon further air injections (in addition to the original 40 air injections), (1) the stage A SHC stopped increasing, and (2) the stage B SHC decreased.

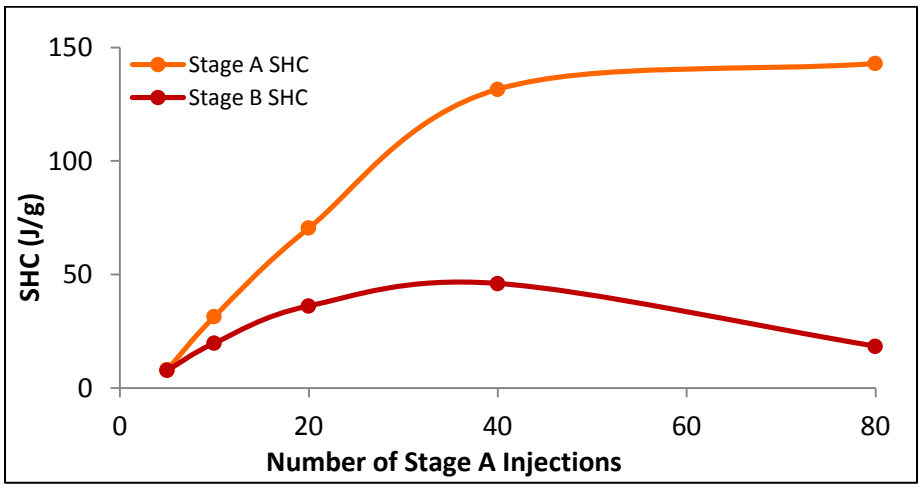

Figure 4-6: SHC as a Function of Number of Stage A Injections: Voisey's Bay Sample, 70°C Test

Figure 4-7 shows SHC generated by the Sudbury sample, plotted against the number of air injections in stage A. Similar to the Voisey's Bay sample, upon initial increase of the number of air injections (10 to 20 cycles), both stage A and stage B SHCs increased. As further air injections were made (20 to 40 cycles), some tests (50°C and 60°C) showed decrease in the stage B SHC.

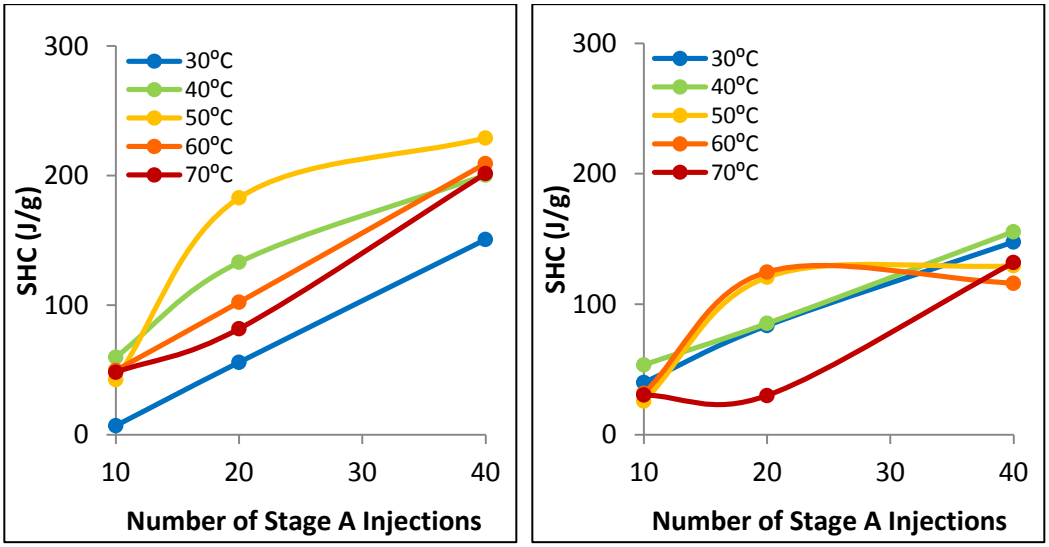

Figure 4-7: SHC as a Function of Number of Stage A Injections, Sudbury Sample: a) Stage A SHCs and b) Stage B SHCs

4.1.2 Elemental Sulfur Formation

The elemental sulfur formed during the weathering in stage A was analysed using carbon disulfide dissolution method (Section 3.4.1). This analytical technique was validated by Jung [15].

Voisey's Bay Sample

Figure 4-8 shows the elemental sulfur generated by the Voisey's Bay sample, plotted against the number of stage A air injections. Generation of elemental sulfur was observed to increase with (1) increasing number of air injections and (2) increasing temperatures in stage A, with the exceptions observed in the 70°C-test. Less elemental sulfur was generated at 70°C, compared to that generated at lower temperatures.

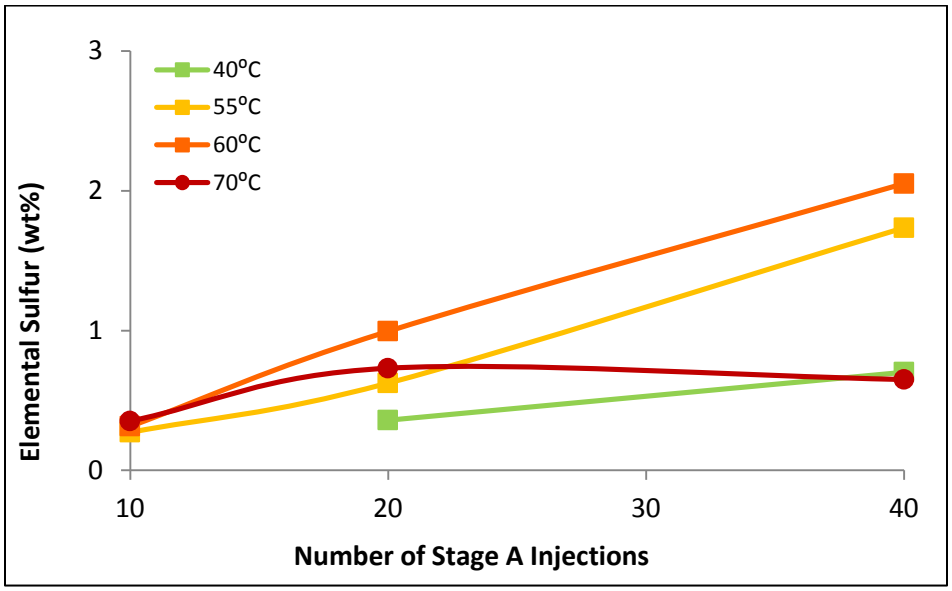

Figure 4-8: Elemental Sulfur Formation as a Function of Number of Stage A Injections, Voisey's Bay Sample

Sudbury Sample

Figure 4-9 shows the elemental sulfur generated by the Sudbury sample, plotted against the number of stage A air injections. Similar to the Voisey's Bay sample,

an increase in the elemental sulfur generation was observed with (1) increasing number of stage A air injections, and (2) increasing stage A temperatures, with the exceptions observed in the 70°C-tests. Less elemental sulfur was generated at 70°C, compared to that generated at lower temperatures: results from the 40 cycle tests shows 2.5% elemental sulfur was produced at 60°C, compared to 1.3% elemental sulfur at 70°C.

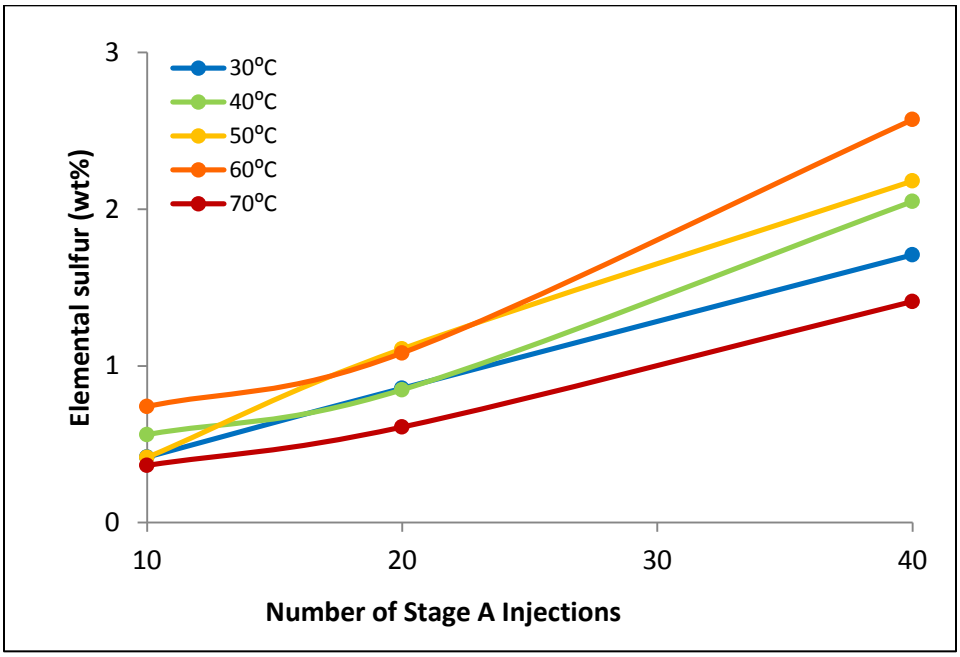

Figure 4-9: Elemental Sulfur Formation as a Function of Number of Stage A Injections, Sudbury Sample

4.1.2.1 Suspected Reason for Lower Elemental Sulfur Generation at 70°C

Both the Voisey's Bay and the Sudbury samples showed the 70°C-tests did not follow the trend with temperature given by the 40-60 °C tests (Figure 4-8 and Figure 4-9); less elemental sulfur was generated than the projected values. The

argument advanced was that at the higher temperature (70°C) the standard stage A airflow rate (100mL/min) may not be sufficient for the sample to oxidize as completely as it does at the lower temperatures (See Section 5) and thus results in less elemental sulfur being produced. To test whether an increased airflow rate increases the elemental sulfur generation, additional tests were conducted at 70°C with airflow rate raised to 300mL/min and the results were added to the data set.

Figure 4-10 shows the results obtained from the Voisey's Bay sample tested at 70°C, at 300mL/min and 100mL/min. When tested at 300mL/min, more elemental sulfur was generated, compared to that generated at 100mL/min.

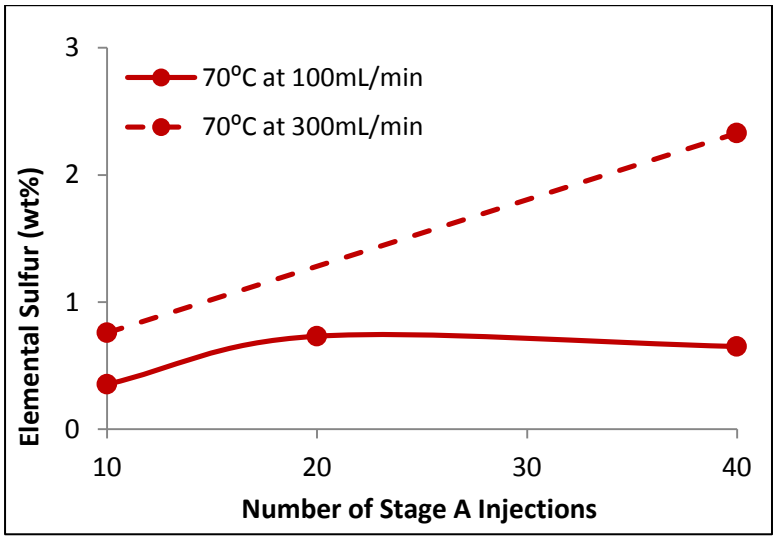

Figure 4-10: Elemental Sulfur Formation as a Function of Number of Stage A Injections, Voisey's Bay Sample in 70°C test: at 100mL/min and 300mL/min

Figure 4-11 shows the elemental sulfur generated by the Sudbury samples, at both airflow rates of 100mL/min and 300mL/min, plotted against the number of stage

A air injections. For the samples weathered for 10 and 20 air injections, more elemental sulfur was generated at 300mL/min, compared to that generated at 100mL/min. When weathered for 40 air injections, however, less elemental sulfur was generated at 300mL/min. While the argument that more air is needed at the higher temperature is supported to some extent there still appears to be another unknown factor controlling sulphur production.

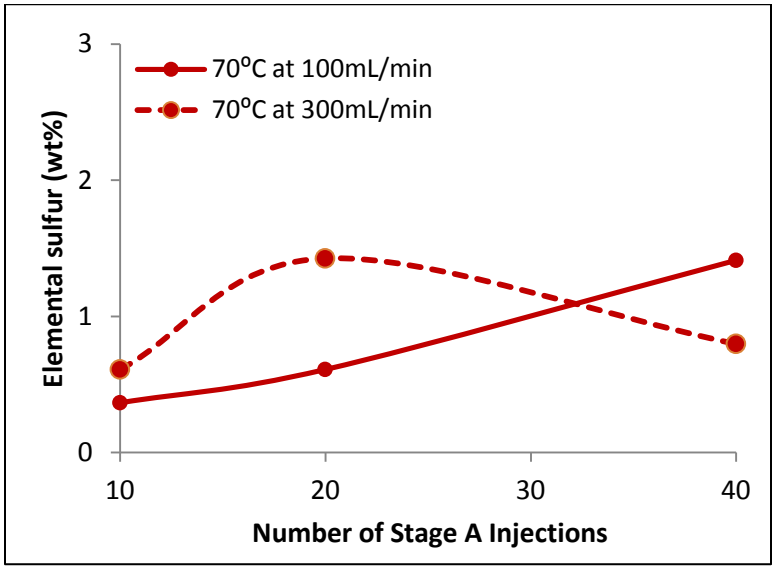

Figure 4-11: Elemental Sulfur Formation as a Function of Number of Stage A Injections, Sudbury Sample in 70°C test: at 100mL/min and 300mL/min

4.1.4 Elemental Sulfur and Stage B Self-heating

Figure 4-12 shows the stage B SHCs generated by the Voisey's Bay sample, plotted against the elemental sulfur generated during the weathering stage (stage A). The SHC generally increased with the increase in the elemental sulfur, with the exception observed in the 70°C-tests. Samples weathered at 70°C sometimes generated a higher SHC with less elemental sulfur: 0.7% elemental sulfur produced 45J/g SHC B, compared to 0.75% elemental sulfur producing 35J/g SHC.

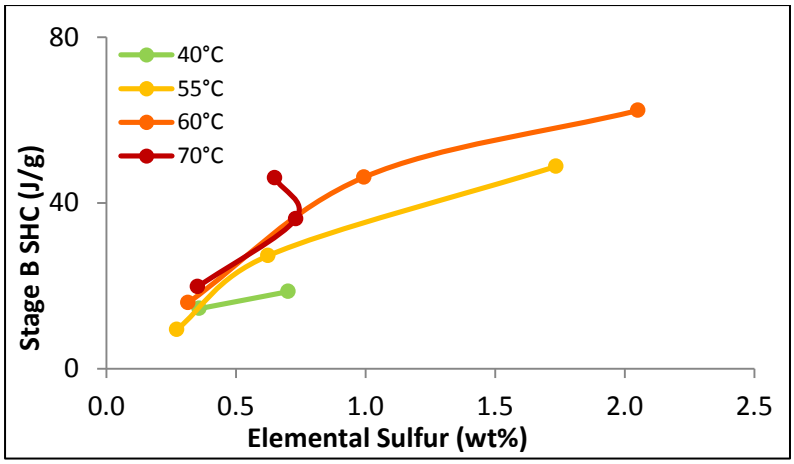

Figure 4-12: Elemental Sulfur and Stage B SHC, Voisey's Bay Sample

Figure 4-13 shows the stage B SHC generated by the Sudbury sample, plotted against the elemental sulfur generated during the weathering stage (modified stage A). For the samples weathered at lower temperatures (30 and 40°C), the correlation between the elemental sulfur and stage B SHC is observed to be linear. For the samples weathered at higher temperatures (50, 60 and 70°C), however, the correlation is non-linear.

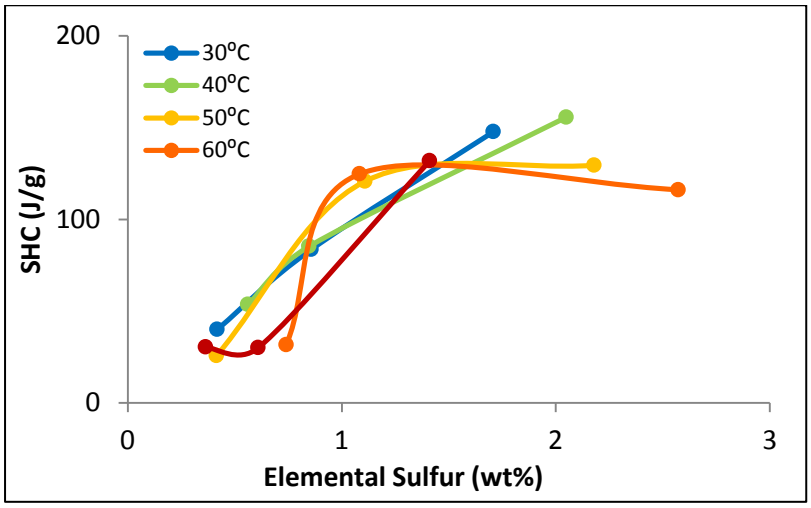

Figure 4-13: Elemental Sulfur and Stage B SHC, Sudbury Sample

Figure 4-14 shows the scatter plot of the Figure 4-12 and Figure 4-13 data. The correlation between the elemental sulfur and stage B SHC is observed to be non-linear, for both the Voisey's Bay sample (Figure 4-14-a) and the Sudbury sample (Figure 4-14-b), with the R^2 values of 0.84 and 0.87, respectively.

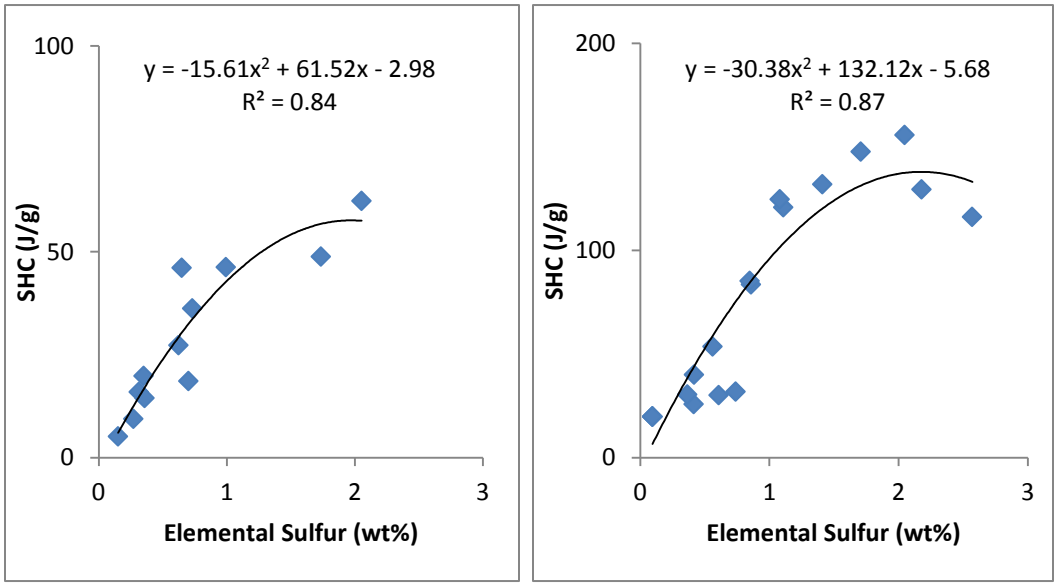

Figure 4-14: Elemental Sulfur and Stage B SHC (Scattered): a) Voisey's Bay Sample and b) Sudbury Sample

4.2 Elemental Sulfur Generation During Induction Period (Delay)

As noted in Section 1.1.3.1, some materials exhibit an induction period (delay) in the onset of self-heating in stage A. The length of the delay depended on several factors, including the sample type and temperatures; the Voisey's Bay sample exhibited the longest delay at 40°C, and the Sudbury sample the longest delay at 30°C (Section 4.1.1.1). The Voisey's Bay and the Sudbury samples were tested at

40°C and 30°C, respectively, to investigate (1) the generation of elemental sulfur during the delay, and (2) the resulting stage B SHC.

Voisey Bay's Sample

Figure 4-15 shows the thermogram response of the Voisey's Bay sample during a 20-cycle test at 40°C, followed by stage B. The initiation of self-heating required 16 cycles, prior to the 4 just measurable self-heating peaks in stage A. The sample obtained after the 20 cycles of stage A contained 0.36% of elemental sulfur, which resulted in 15J/g stage B SHC.

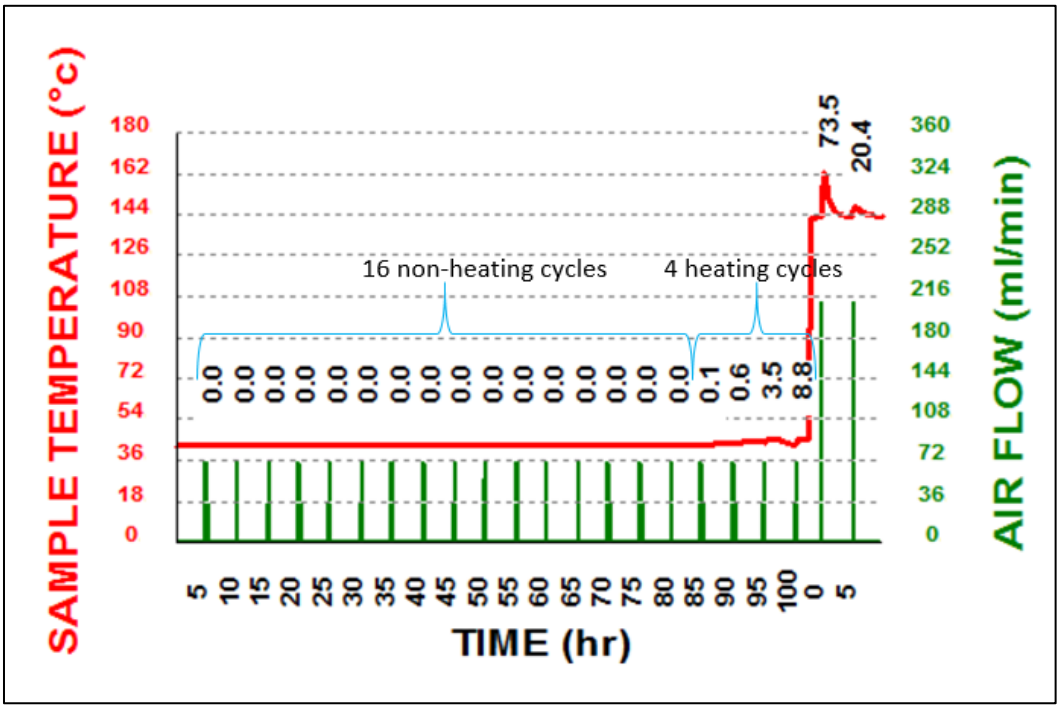

Figure 4-15: Thermogram Response: Voisey's Bay Sample in 40°C test (20 Cycles)

Figure 4-16 shows the thermogram response of the Voisey's Bay sample during a 16-cycle test at 40°C, followed by stage B; stage A was stopped immediately after the 16 cycles of the non-heating period. The sample obtained after the 16 cycles of stage A contained 0.15% of elemental sulfur, which resulted in 5J/g stage B SHC.

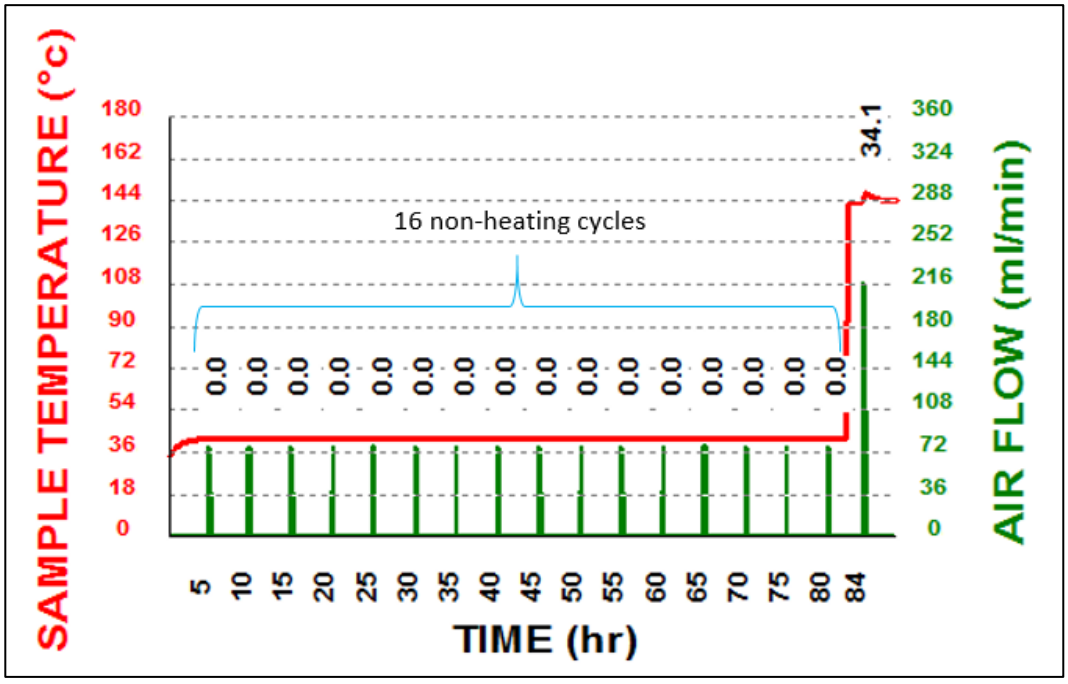

Figure 4-16: Thermogram Response: Voisey's Bay Sample in 40°C Test (16 Cycles)

As a baseline, the as-received Voisey sample was tested for stage B SHC (i.e., the sample was directly tested in stage B, without weathering in stage A). The sample originally contained 0.03% of elemental sulfur, which resulted in 2J/g of stage B SHC.

Sudbury Sample:

Figure 4-17 shows the thermogram response of the Sudbury sample during a 10-cycle test at 30°C, followed by stage B. The initiation of self-heating required 7 cycles prior to the 3 self-heating peaks in stage A. The sample obtained after the 10 cycles of stage A contained 0.42% of elemental sulfur, which resulted in 40J/g stage B SHC.

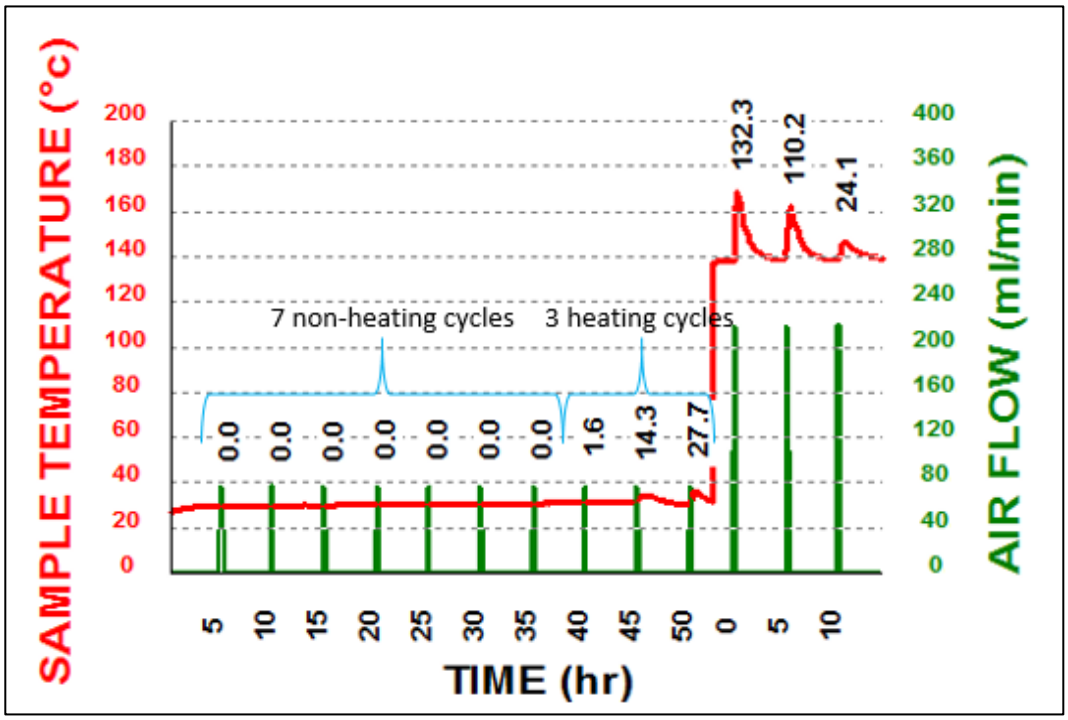

Figure 4-17: Thermogram Response: Sudbury Sample in 30°C Test (10 Cycles)

Figure 4-18 shows the thermogram response of the Sudbury sample during a 7-cycle test at 30°C, followed by stage B; stage A was stopped immediately after the 7 cycles of non-heating period. The sample obtained after the 7 cycles of stage A contained 0.26% of elemental sulfur, which resulted in 26J/g stage B SHC.

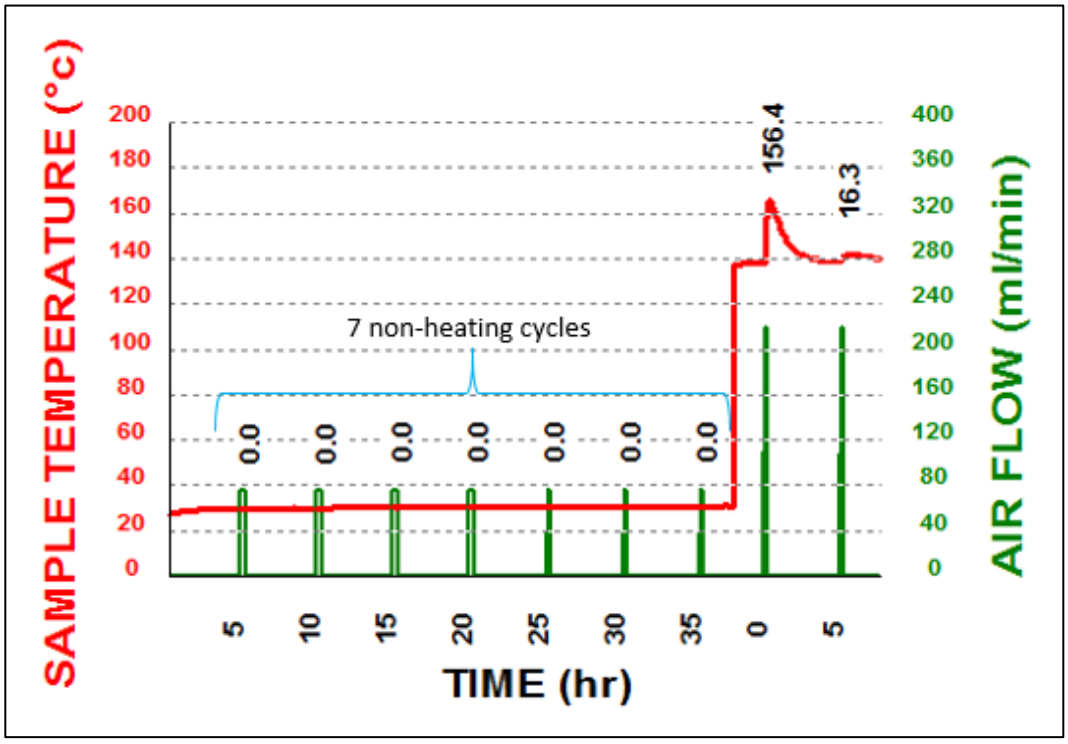

Figure 4-18: Thermogram Response: Sudbury Sample in 30°C Test (7 Cycles)

As baseline, the as-received Sudbury sample was tested for the stage B SHC. The sample originally contained 0.10% of elemental sulfur, which resulted in 20J/g of stage B SHC.

Summary of Results:

Figure 4-19 shows the elemental sulfur and the stage B SHC results obtained from the Voisey's Bay sample, plotted against the number of air injections in stage A. For the elemental sulfur, the as-received sample contained 0.03% of elemental sulfur; a 0.12% of increase was observed after the 16 non-heating cycles, and a 0.21% of additional increase was observed after the 4 heating cycles. For the stage B SHC, the as-received sample produced 3J/g of SHC; 3J/g of increase was observed after the 16 non-heating cycles, and a 10J/g of additional increase was observed after the 4 heating cycles.

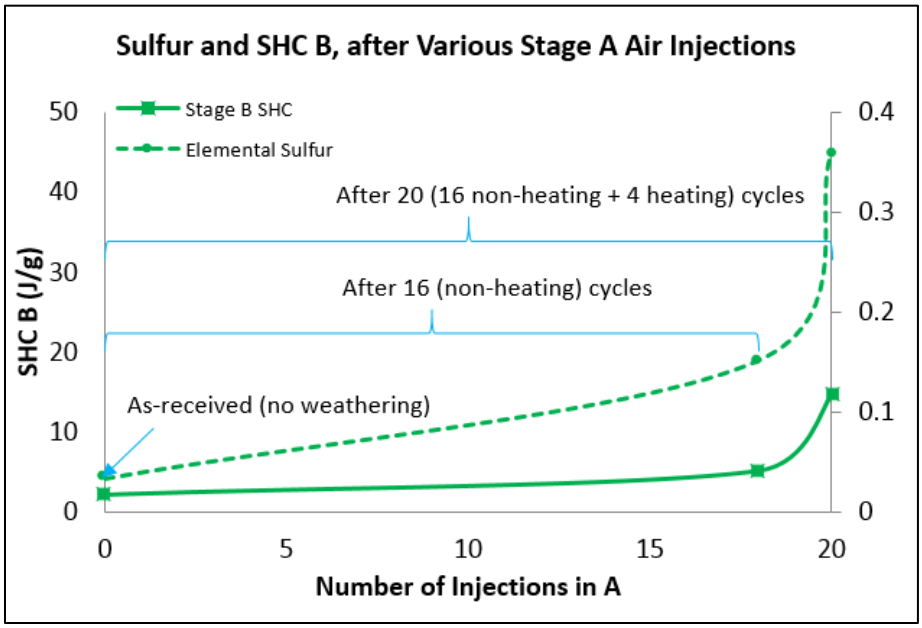

Figure 4-19: Elemental Sulfur and Stage B SHC: Voisey's Bay Sample in 40 °C Test

Figure 4-20 shows the elemental sulfur and the stage B SHC results obtained from the Sudbury sample, plotted against the number of air injections in stage A. For the elemental sulfur, the as-received sample contained 0.10% elemental sulfur; a 0.15% of increase was observed after the 7 non-heating cycles, and a 0.16% of additional increase was observed after the 3 heating cycles. For the stage B SHC, the as-received sample produced 20J/g of SHC; a 6J/g of increase was observed after the 7 non-heating cycles, and a 14J/g of additional increase was observed after the 3 heating cycles.

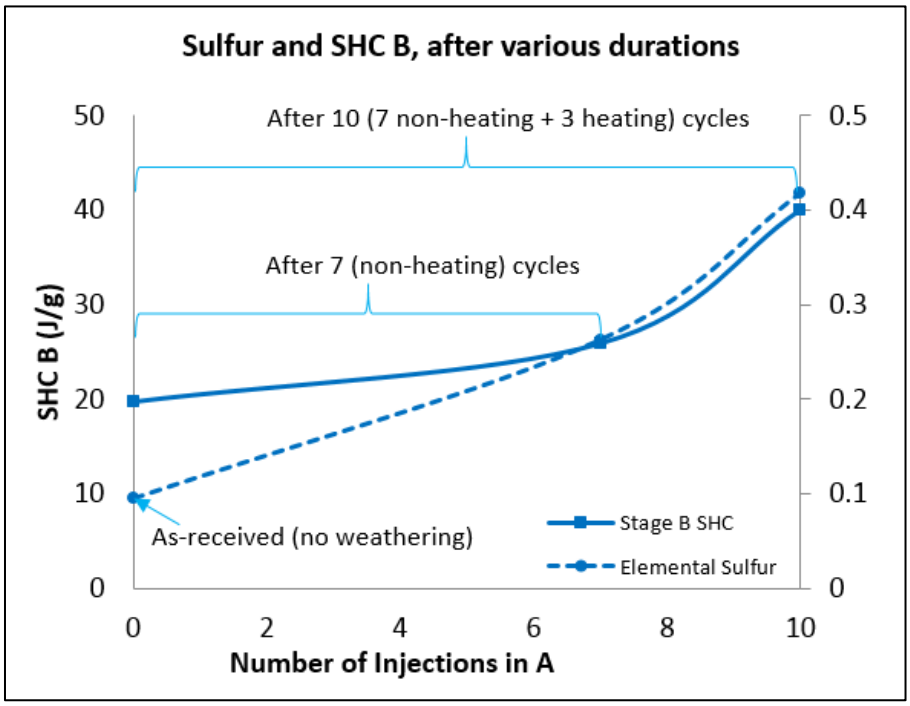

Figure 4-20: Elemental Sulfur and Stage B SHC: Sudbury Sample in 40 °C Test

4.3 Recycle Test Procedure (RTP)

In the recycle test procedure, RTP, a sample is recycled over and over, until no more measurable self-heating is observed (See Section 3.3.3). This is done through a sequence of standard tests, where each one of the sequential tests comprised: (1) stage A testing, (2) elemental sulfur analysis, and (3) stage B testing. The elemental sulfur and the resulting stage B SHC were recorded from each recycle; the results are shown in this section, along with other observations.

4.3.1 Elemental sulfur and Stage B Self-heating

Voisey's Bay Sample

Figure 4-21 shows the elemental sulfur and the stage B SHC generated by the Voisey's Bay sample during an RTP, plotted against the recycle number; this RTP was conducted with stage A airflow rate of 100mL/min. The elemental sulfur generation increased for the first 2 recycles, followed by a rapid decrease on the 3rd recycle and fluctuations until the 11th recycle. The stage B SHC roughly corresponded to the elemental sulfur generation: it reached maximum on the 1st recycle, followed by a rapid decrease until the 4th recycle, and a gradual decrease (with fluctuations) until the 11th recycle. On the 11th recycle, although some elemental sulfur was still generated, no measurable self-heating was observed, and thus the RTP was stopped. A total of 11 recycles were conducted in this RTP, producing 141J/g HGC (Section 3.3.3) with 3.8% cumulative sulfur (total amount of sulfur generated in an RTP).

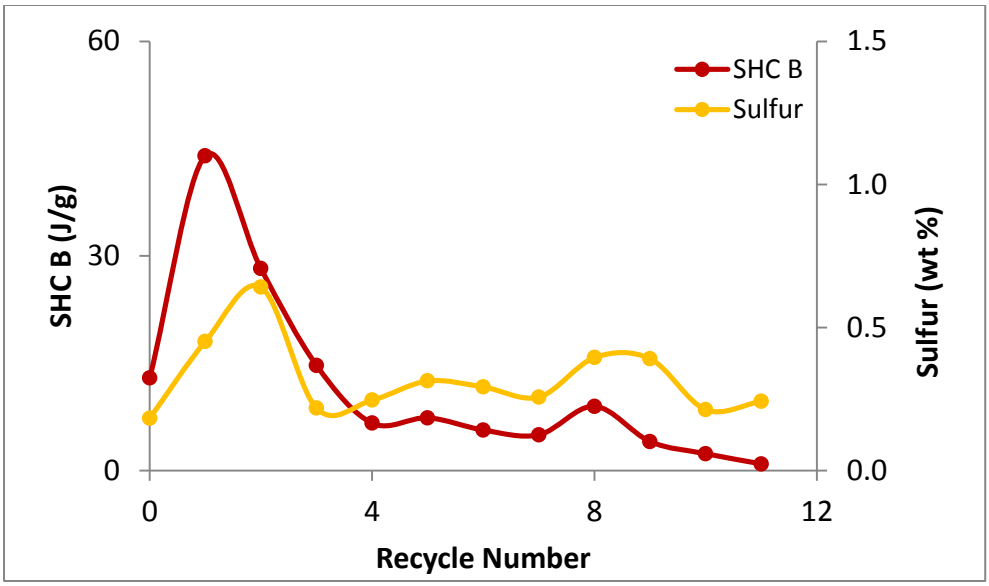

Figure 4-21: RTP at 100mL/min, Voisey's Bay Sample

Figure 4-22 shows the same data as Figure 4-21 but at a stage A airflow rate of 300mL/min. The elemental sulfur generation reached maximum on the 1st recycle, followed by a rapid decrease on the 2nd recycle and fluctuations until the 11th recycle. The stage B SHC roughly corresponded to elemental sulfur generation: the SHC reached the maximum on the initial test, followed by a rapid decrease until the 3rd recycle and fluctuations until the 11th recycle. A total of 11 recycles were conducted in this RTP, producing 239J/g HGC with 5.4% cumulative sulfur.

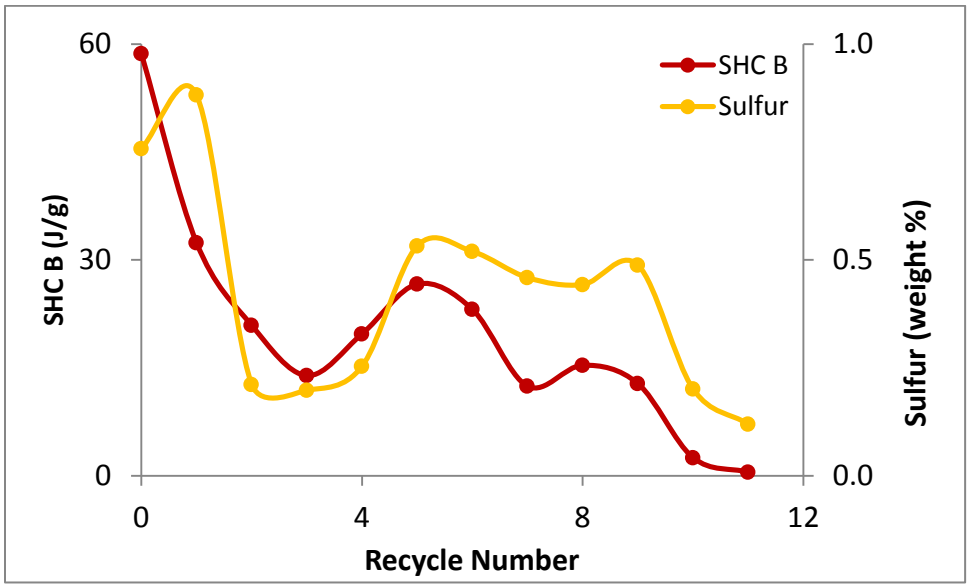

Figure 4-22: RTP at 300mL/min, Voisey's Bay Sample

Sudbury Sample

Figure 4-23 shows the elemental sulfur and stage B SHCs generated by the Sudbury sample during an RTP, plotted against the recycle numbers; this RTP was conducted with stage A airflow rate of 100mL/min. The elemental sulfur generation reached the maximum on the 1st recycle, followed by a gradual decrease until the 6th recycle; a second maximum was then observed at the 8th recycle, followed by another gradual decrease until the 14th recycle. The stage B SHC corresponded to the elemental sulfur generation only during the first and last few recycles: the SHC continuously increased until the maximum was reached on the 6th recycle, and then gradually decreased until the 14th recycle. A total of 14 recycles were conducted in this RTP, producing 689J/g HGC with 4.5% cumulative sulfur.

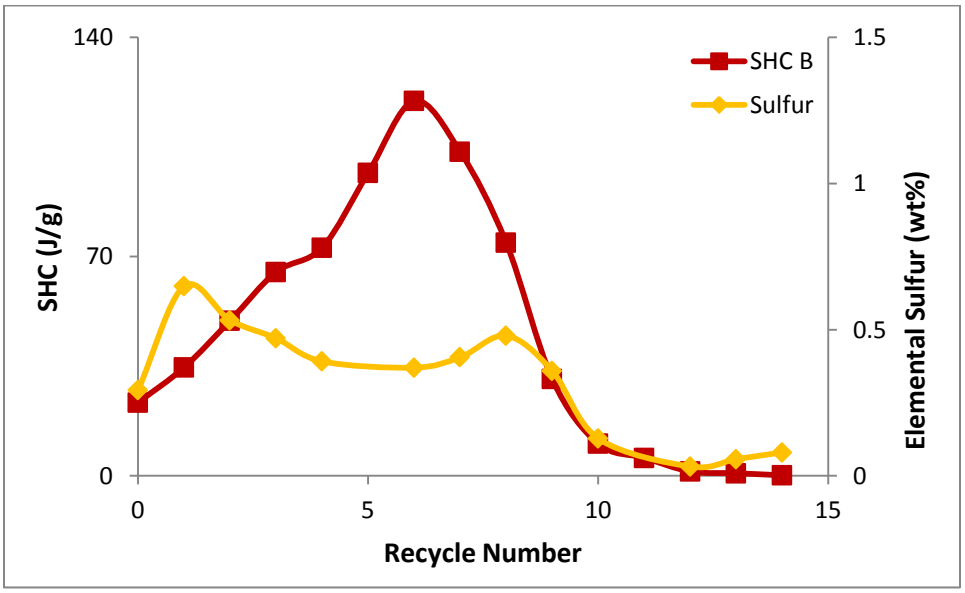

Figure 4-23: RTP at 100mL/min, Sudbury Sample

Figure 4-24 shows the same data as Figure 4-21 with stage A airflow rate of 300mL/min. The elemental sulfur generation reached maximum on the 2nd recycle, followed by a gradual decrease until the 7th recycle. The stage B SHC corresponded to the elemental sulfur generation: the maximum SHC was found on the 2nd recycle, followed by a gradual decrease until the end of the test. A total of 7 recycles were conducted in this RTP, producing 535J/g HGC with 6% cumulative sulfur.

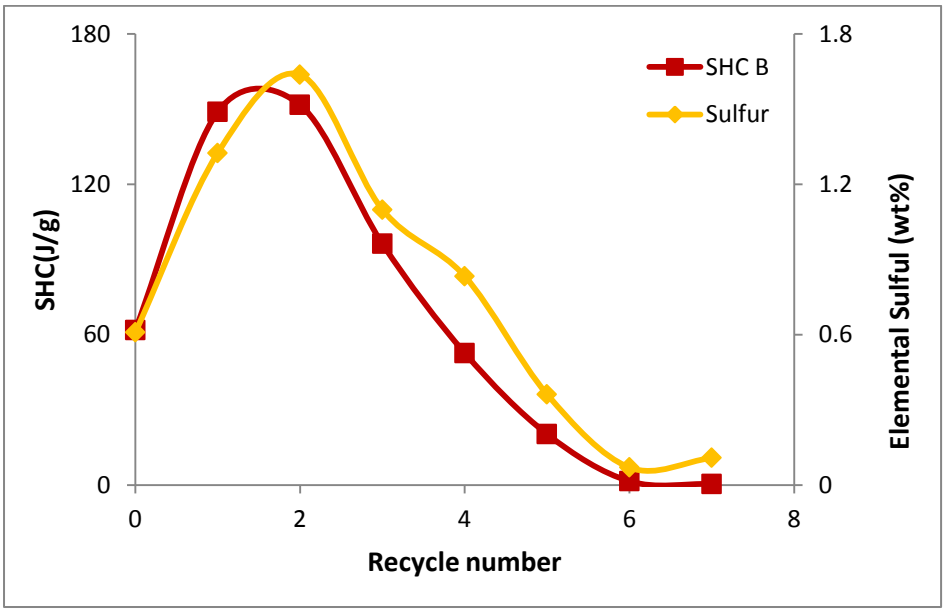

Figure 4-24: RTP at 300mL/min, Sudbury Sample

Single Mineral Specimens and Mixtures

The RTPs were also conducted with the following 3 mixtures (Section 3.1.2):

- Sample 1: 20% Pyrrhotite – 80% Sand
- Sample 2: 20% Pyrrhotite – 80% Pyrrhotite

- Sample 3:100% Pyrite

For these samples, the RTPs were conducted with stage A airflow rate of 100mL/min only.

Figure 4-25 shows the elemental sulfur and the stage B SHC generated by Sample 1 during an RTP, plotted against the recycle numbers. The elemental sulfur generation gradually increased until the 3rd recycle, followed by a gradual decrease until the 6th recycle. The stage B SHC corresponded to the elemental sulfur generation: SHC reached maximum on the 3rd recycle, followed by a gradual decrease until the 6th recycle. A total of 6 recycles were conducted in this RTP, producing 212J/g HGC with 2% cumulative sulfur.

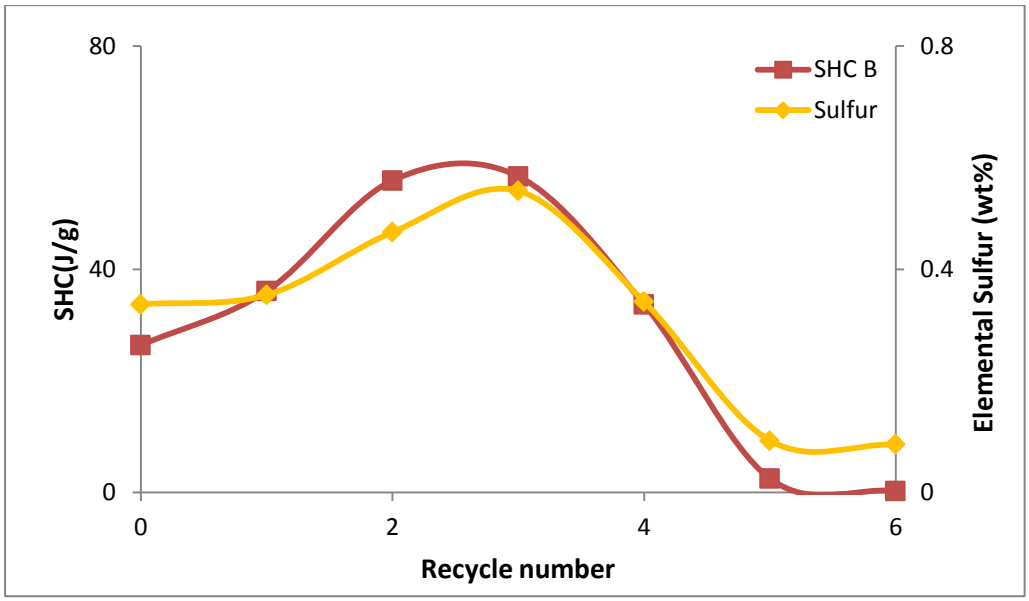

Figure 4-25: RTP at 100mL/min, Sample 1

Figure 4-26 shows the elemental sulfur and the stage B SHC generated by Sample 2 during an RTP, plotted against the recycle number. The elemental sulfur increased until the 2nd recycle, followed by a rapid decrease on the 3rd recycle and a gradual decrease until the 5th recycle. The stage B SHC corresponded to the elemental sulfur generation: it reached maximum on the 2nd recycle, followed by a rapid decrease on the 3rd recycle and a gradual decrease until the 7th recycle. Total of 7 recycles were conducted in this RTP, producing 268J/g HGC with 1% cumulative sulfur.

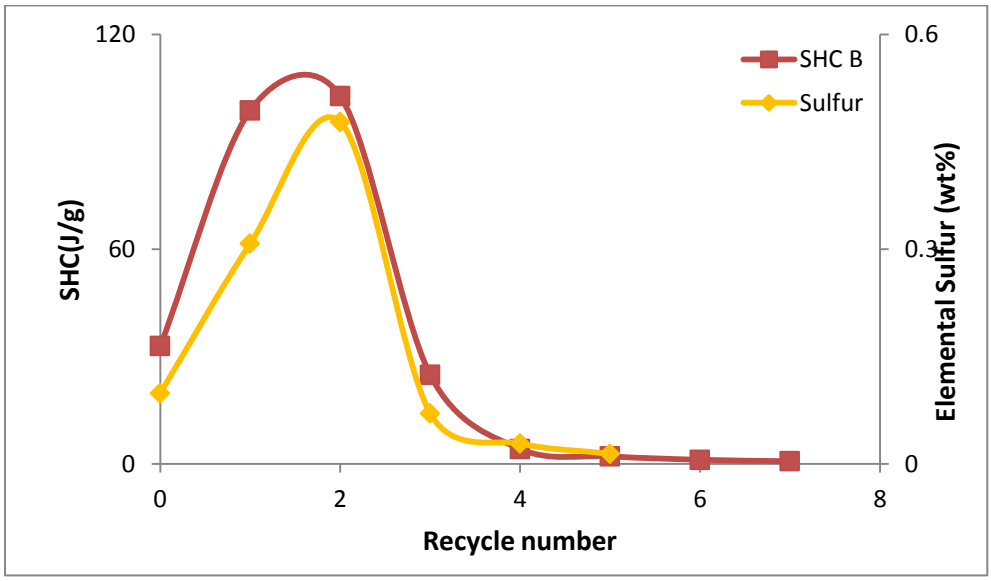

Figure 4-26: RTP at 100mL/min, Sample 2

Figure 4-27 shows the elemental sulfur and the stage B SHCs generated by Sample 3 during an RTP, plotted against the recycle numbers. This sample produced negligible elemental sulfur, and thus showed minimal heating in stage B. Total of 2 recycles were conducted in this RTP, producing 3J/g HGC with 0.1% cumulative sulfur.

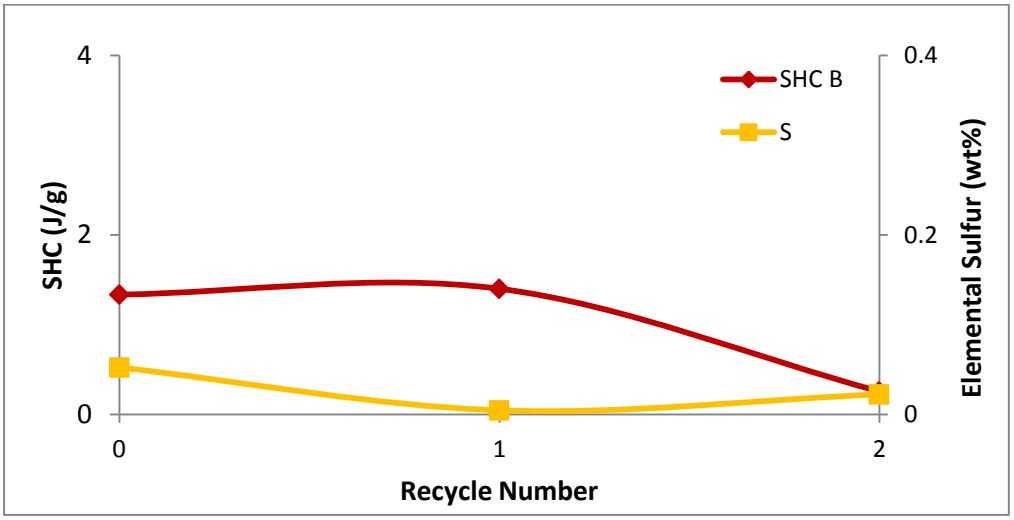

Figure 4-27: RTP at 100mL/min, Sample 3

4.3.3 HGC and Total Sulfur

Table 4-1 summarizes the results obtained from all RTP tests conducted with stage A airflow rate of 100mL/min. For most samples, the stage B SHC corresponded with the elemental sulfur generated in each recycle. The HGC, however, was not directly proportional to the cumulative amount of elemental sulfur, i.e., higher cumulative sulfur did not necessarily produce higher HGC.

Table 4-1: Summary – All RTPs conducted at 100mL/min

Sample	∑ S° (%)	HGC B (J/g)	Correlation S vs. SHC B	# Recycle upon completion
Voisey's Bay	3.8	141	Yes	11
Sudbury	4.7	689	Partial	14
Sample 1	2.0	212	Yes	5
Sample 2	1.1	268	Yes	6
Sample 3	0.1	3	Yes	2

Table 4-2 summarizes the results from the Voisey's Bay and the Sudbury samples, conducted at both stage A airflow rates of 100mL/min and 300mL/min. The Voisey's Bay sample produced a substantially higher HGC at 300mL/min (239J/g) than at 100mL/min (141J/g), whereas the Sudbury sample produced a higher HGC at 100mL/min (689J/g) than at 300mL/min (534J/g); both samples generated less elemental sulfur at 300mL/min. For the Sudbury sample, the

correlation between the elemental sulfur and the stage B SHC was better at 300mL/min, than at 100mL/min.

Table 4-2: Summary – Voisey's Bay and Sudbury RTPs at 100mL/min and 300mL/min

Sample	Airflow rate (mL/min)	∑ S° (%)	HGC B (J/g)	Correlation S vs. SHC B	# Recycle upon completion
Voisey's Bay	100	5.7	141	Yes	12
Voisey's Bay	300	5.4	239	Yes	11
Sudbury	100	4.7	689	Partial	14
Sudbury	300	6.2	534	Yes	7

4.3.4 An Observation: Temperature Increase upon Water Addition

As described in Section 3.3.3, a RTP involves a step in which the samples are remoistened prior to the next recycle test. During this step, it was observed that the sample temperature immediately increased upon the addition of water; the maximum temperature reached by the samples was recorded from each remoistening procedure.

Figure 4-28 shows the maximum temperature reached by the Voisey's Bay and the Sudbury samples upon remoistening prior to each recycle test. The Voisey's Bay sample temperature reached as high as 39°C (6^{th} recycle in 100mL/min RTP), and the Sudbury sample temperature reached as high as 46°C (5^{th} recycle in

100mL/min RTP). For both samples, the temperatures were generally higher when the RTPs were conducted at 100mL/min, than at 300mL/min.

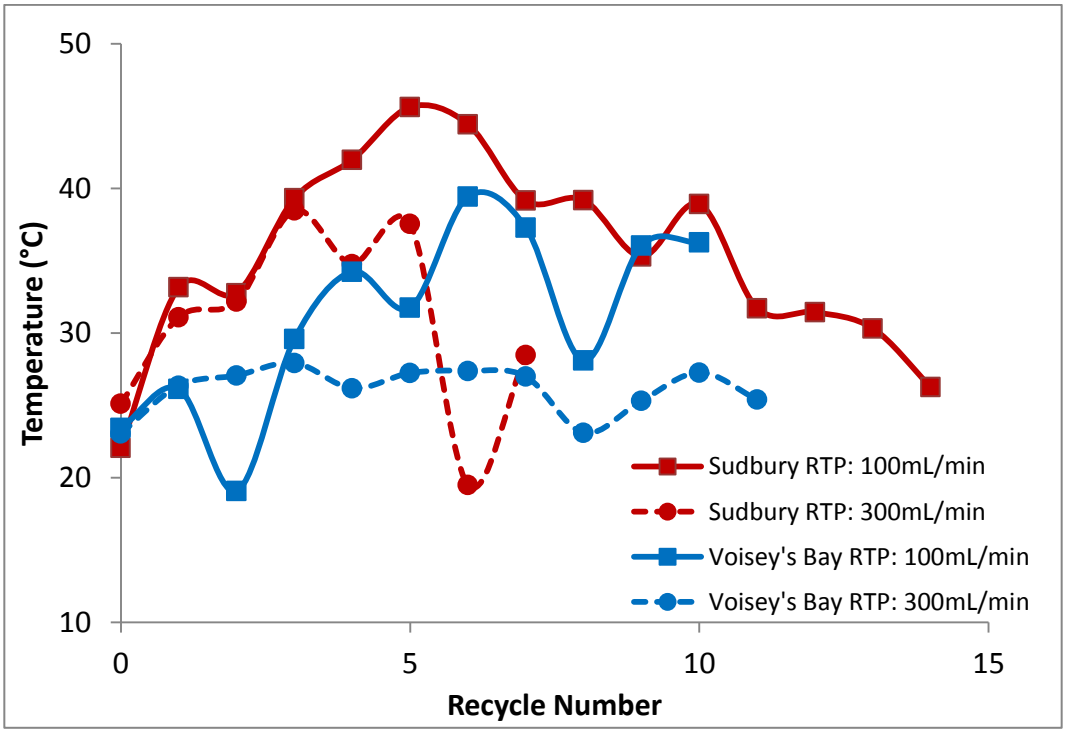

Figure 4-28: Maximum Temperature Reached Upon Remoistening: Voisey's Bay and Sudbury Samples

Figure 4-29 shows the maximum temperatures reached by Sample 1, Sample 2 and Sample 3 upon remoistening prior to each recycle test. Sample 1 temperature reached as high as 33°C (5th recycle), whereas Sample 2 temperature reached as high as 38°C (4th recycle). Sample 3 temperature reached as high as 24°C (2nd recycle).

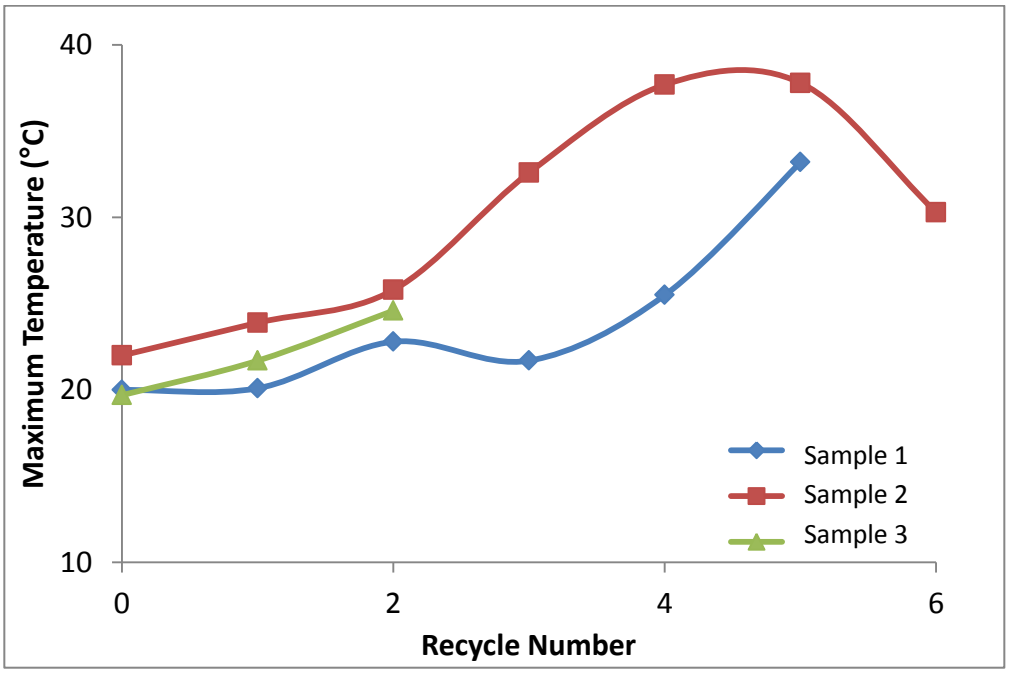

Figure 4-29: Maximum Temperature Reached Upon Remoistening: Sample 1, 2 and 3

4.4 Analysis of Samples

4.4.1 XRD Results

4.4.1.1 XRD Results – Samples from Weathering Tests

Table 4-3 shows the XRD results obtained from representative Sudbury samples: the "fresh" (as-received) sample and the weathered samples from the 40°C and the 50°C tests were selected for the composition analysis.

Table 4-3: XRD Results – Selected Sudbury Samples from Weathering Tests

Weathering condition	Fe_7S_8	SiO_2	Fe_3O_4	$NaCaAlSiO_8$	FeO(OH)
As received	√	√	√	√	
10 cycles at 40°C	√	√	√	√	
20 cycles at 40°C	√	√	√	√	√
40 cycles at 40°C	√	√	√	√	√
40 cycles at 40°C followed by stage B	√	√	√	√	√
10 cycles at 50°C	√	√	√	√	
20 cycles at 50°C	√	√	√	√	
40 cycles at 50°C	√	√	√	√	√

The fresh sample was composed of pyrrhotite, magnetite and silicates. When the sample was weathered for 10 cycles at 40°C, no change was observed in the composition; however, when the sample was weathered for 20 and 40 cycles at 40°C, the sample showed presence of goethite. Similarly, the samples from the

50°C-tests showed no change in composition after 10 and 20 cycles of weathering, however, they showed presence of goethite after 40 cycles of weathering.

The stage B-tested sample (after 40 cycles of weathering at 40°C) showed no change in the composition, compared to the stage A-tested sample (40 cycles at 40°C).

4.4.1.2 XRD Results – Samples from RTP Tests

Table 4-4 shows the XRD results obtained from representative Sudbury samples; the fresh sample and the samples after the 1st, 7th and the 15th recycles were selected for the composition analysis.

Table 4-4: XRD Results – Selected Sudbury Samples from RTPs

Recycle #	Fe_7S_8	SiO_2	Fe_3O_4	$NaCaAlSiO_8$	$FeO(OH)$	$FeSO_4 \cdot (7H_2O)$
As received	√	√	√	√		
1	√	√	√	√		
7	√	√	√	√	√	√
15		√		√	√	√

The fresh sample was composed of pyrrhotite, magnetite and silicates. When the sample was recycled for the first time, no change was observed in the composition; however, after the 7th recycle, the sample showed a presence of goethite and iron sulphate hydrates. After the 15th recycle, i.e., upon completion of the RTP,

pyrrhotite and magnetite were no longer observed: the sample was only composed of goethite, iron sulphate hydrates and silicates.

4.4.2 XPS Results

Selected Sudbury samples were analysed by XPS to generate sulfur (2p) photoelectron spectra; Table 4-5 lists the reference peak binding energies ($2p_{3/2}$) used for initial peak fitting, prepared by Pratt [48]. For polysulphide (S_n^{2-}), the reference peak binding energy (2p) used for initial peak fitting was 163.6 eV [49].

Table 4-5: Reference Peak Binding Energies of Surface Sulfur Species [48]

S(2p) Species	Binding Energy ($2p_{3/2}$)	Reference
Monosulphide (S^{2-})	161.3	Pratt et al. 1994 [48]
Disulphide (S_2^{2-})	162.5, 162.3	Mycroft et al 1990 [50], Pratt et al. 1994 [48]
Elemental Sulfur (S_8)	164.2	Carlson 1975 [51]
Sulfite (SO_3^{2-})	166.4	Wagner et al. 1979 [52]
Sulfate (SO_4^{2-})	168.5	Jones et al. 1992 [53]

4.4.2.1 As-received Sample

Figure 4-30 illustrates the spectrum of the as-received Sudbury sample, fitted with doublets. The sample mainly consisted of sulfate, hydrated sulfate, polysulphide, disulphide and monosulphide, indicated by the peaks at 168.7, 167.3, 163.8, 162.4 and 161.4eV, respectively. Sulfates (sulfate and hydrated sulfate) comprise 76% of the total sulfur, and the sulphides (monosulphide, disulphide and polysulphide)

consistute the other 24%. Within the sulphide region (161-165eV), polysulphides are the most predominant (163.8eV), followed by monosulphide (161.4eV) and disulphide (162.4eV); the predominance of polysulphide is indicated by the local maximum in the fitted curve (summation curve).

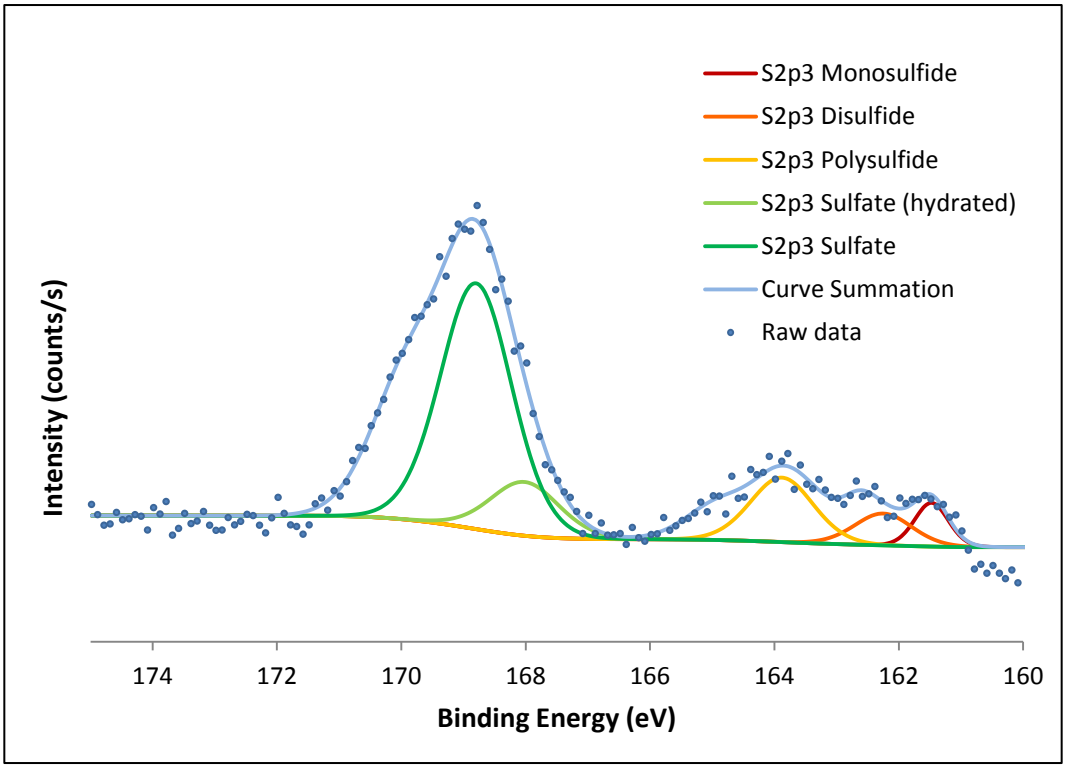

Figure 4-30: XPS: S (2p) Spectrum of an As-received Sudbury Sample

4.4.2.2 Samples from Weathering Tests

The Sudbury samples from the 20 cycle and the 40 cycle tests (conducted at 40°C and 50°C) were analysed using XPS; for each sample, two locations of the same sample were analysed to show consistency of results.

Figure 4-31 presents the results obtained from the 20 cycle test conducted at 40°C; the stage A-tested and the stage B-tested samples are compared to the as-received sample (4.5.2.1). For all three samples, the largest peak was observed at 168.8eV, indicating the predominance of sulphates. Smaller peaks were observed in the range of 161~164 eV, corresponding to sulphides. Within the sulphide region (161~164eV), both the as-received and the stage A-tested samples showed a local maximum at 163.8eV, indicating a predominance of polysulphides. The stage B-tested sample showed a decrease in the sulphide peaks; a local maximum is observed around 162.5eV, which appears to be disulphide.

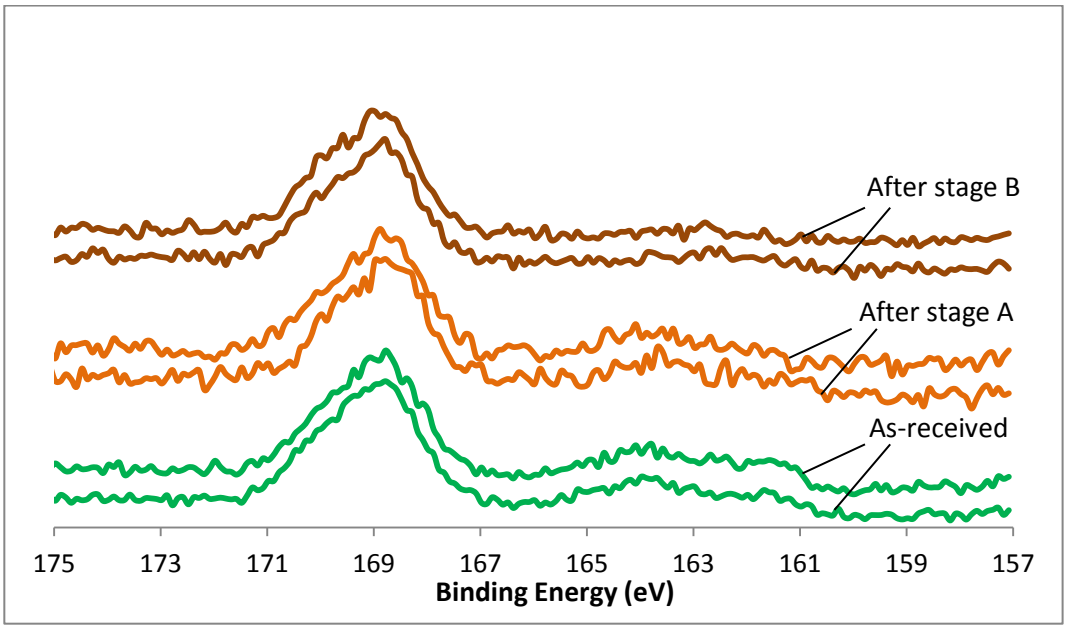

Figure 4-31: S (2p) Spectrum of Sudbury Samples from 20 cycle test at 40°C: As-received, After Stage A and After Stage B

Figure 4-32 presents the results from the 40-cycle test conducted at 40°C. For all three samples, the largest peak was at 168.8eV, indicating the predominance of sulphates. Smaller peaks were observed in the range of 161~164 eV, indicating sulphides. Within the sulphide region (161~164eV), the as-received sample showed a local maximum at 163.8eV. After the sample was tested in stage A, the local maximum shifted to 162.6eV, indicating a dominance of disulphides. When the stage-A tested sample was tested in stage B, the overall sulphide peak decreased, however, the local maximum was still located at 162.6eV.

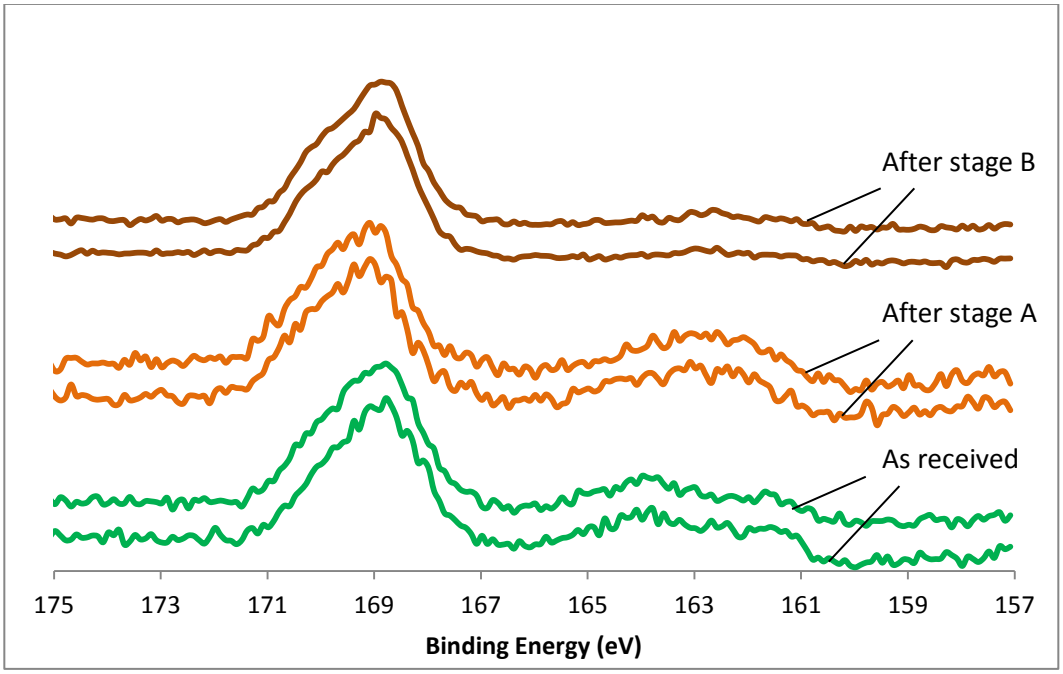

Figure 4-32: S (2p) Spectrum of Sudbury Samples from 40 cycle test at 40°C: As-received, After Stage A and After Stage B

Figure 4-33 and Figure 4-34 presents the results obtained from the 20 and 40 cycle tests conducted at 50°C. Similar to the results obtained from the 40 cycle-test conducted at 40°C (Figure 4-32), the results showed a shift in the local maximum (from polysulphide to disulphide region) after stage A, and a decrease in the overall sulphides during stage B.

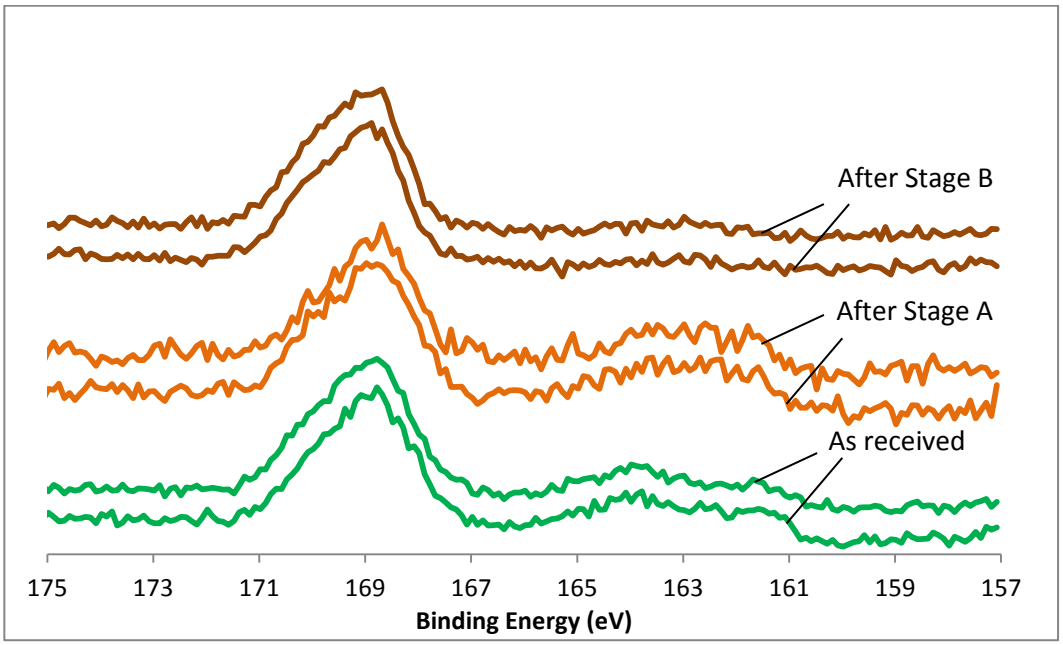

Figure 4-33: S (2p) Spectrum of Sudbury Samples from 20 cycle test at 50°C: As-received, After Stage A and After Stage B

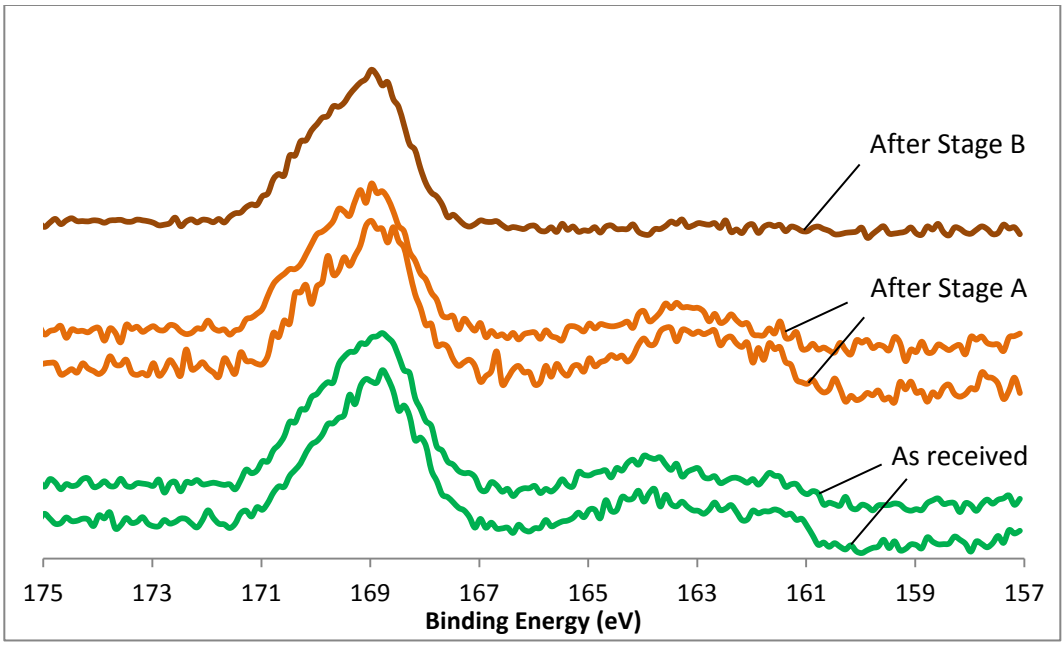

Figure 4-34: S (2p) Spectrum of Sudbury Samples from 40 cycle test at 50°C: As-received, After Stage A and After Stage B

4.4.2.3 Samples from Recycle Tests

The Sudbury samples from the 4th, 7th and the 10th recycles of the 100mL/min RTP test were analysed using XPS; for each sample, two locations of the same sample were analyzed to show consistency of results.

Figure 4-35 presents the results from the 4th recycle test. For both the stage A-tested and the stage B-tested samples, the largest peak was observed at 168.8eV, indicating the predominance of sulphates. Smaller peaks were observed in the range of 161-164 eV, indicating sulphides. Within the sulphide region (161-164eV), the stage A-tested sample showed a local maximum around 162.7eV,

indicating the dominance of disulphide. The stage B-tested sample showed a decrease in the peak, however, the local maximum was still located at 162.7eV.

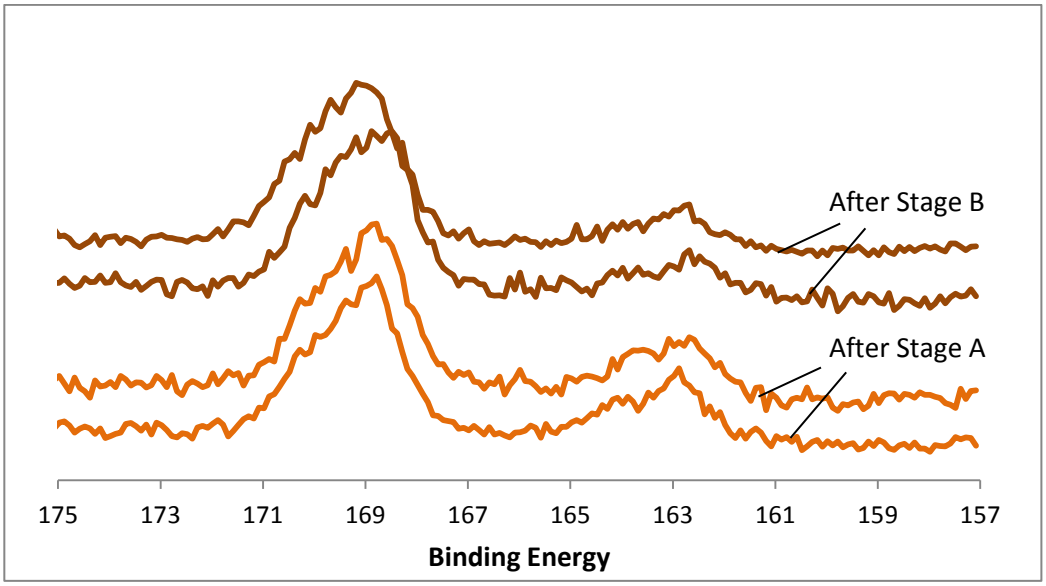

Figure 4-35: S (2p) Spectrum of Sudbury Samples Obtained from 100mL/min RTP, 4th Recycle: After Stage A and After Stage B

Figure 4-36 and Figure 4-37 presents the results from the 7th and the 10th recycle tests. Similar to the results obtained from the 4th recycle test, all samples showed the largest peak at 168.8eV (sulphate) and smaller peaks in the range of 161-164 eV (sulphide), with the local maximum located around 162.7eV. As the samples went through more recycles, the sulphide peak became narrower and smaller.

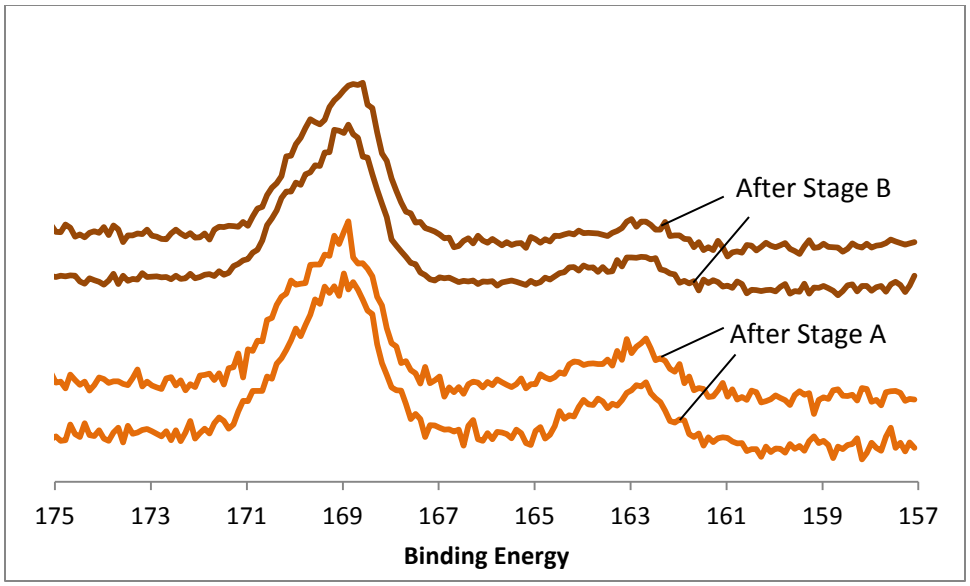

Figure 4-36: S (2p) Spectrum of Sudbury Samples Obtained from 100mL/min RTP, 7th Recycle: After Stage A and After Stage B

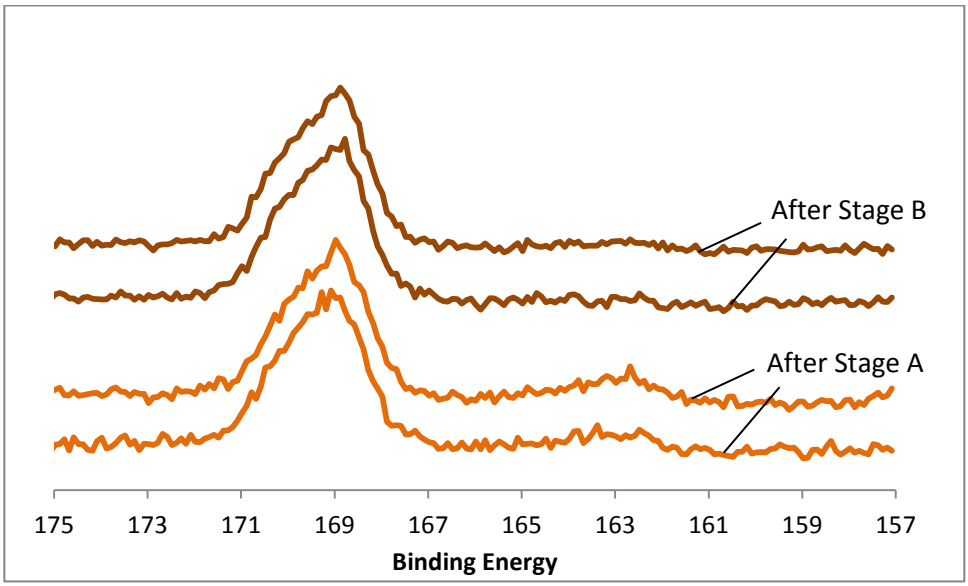

Figure 4-37: S (2p) Spectrum of Sudbury Samples Obtained from 100mL/min RTP, 10th Recycle: After Stage A and After Stage B

4.4.3 Microprobe Results – Samples from Weathering Tests

Table 4-6 shows the Microprobe results obtained from the Sudbury samples: the as-received and the 40°C tested samples (10 and 40 cycles) were selected for the analysis. For each sample, 15 pyrrhotite particles were selected for the Fe and S compositions.

Table 4-6: Fe and S Percentages in Pyrrhotite Particles

Sample	Fe % in Po	S % in Po	Fe:S
As-received	45.9	53.3	0.86
40°C, 10 cycles in A	45.9	53.3	0.86
40°C, 40 cycles in A	46.2	53.1	0.87

The as-received sample showed a Fe:S ratio of 0.86 for the pyrrhotite particles. After the sample was tested for 10 cycles at 40°C, no change was observed in the Fe:S ratio; however, when the sample was tested for 40 cycles at 40°C, a slight increase in the Fe:S ratio was observed, which may or may not be significant.

4.4.4 ICP Results – Samples from RTP Tests

Table 4-7 shows the ICP results of the Sudbury samples obtained from the 100mL/min RTP test; the as-received, stage A tested (from the 4^{th}, 7^{th}, 10^{th} recycles) and stage B tested (from the 4^{th}, 7^{th}, 10^{th} recycles) samples were selected for the determination of Fe and S. As the sample went through the number of recycles, 1) a decrease in the iron and sulfur content, and 2) an increase in the Fe:S ratio were observed.

Table 4-7: Fe and S Percentages in Selected Sudbury Samples

Recycle number	Stage	Fe (wt%)	S (wt%)	Fe:S
As received	N/A	29.9	20.2	1.48
4	A	26.7	17.4	1.54
4	B	25.1	17.3	1.45
7	A	22.5	14.2	1.58
7	B	21.8	13.4	1.63
10	A	19.3	11.3	1.71
10	B	18.3	10.5	1.74

5 Summary and Discussions

This Chapter is divided into three sections. Sections 5.1 and 5.2 are the summary of the results from Sections 4.1, 4.2 and 4.3. Section 5.3 discusses the reaction products from the self-heating of pyrrhotite.

5.1 Effect of Weathering on Self-heating

It has been shown that the conditions in Stage A (degree of weathering) of a sample, increasing sample temperature and number of air injections has an impact on self-heating. Increasing the number of air injections always increased elemental sulfur formation and self-heating in stage B; however, temperature showed a mixed response: For stage A, increasing the temperatures from 40 to ~55°C generally increased elemental sulfur formation and the self-heating in stage B; however, further increasing the temperature from ~55 to 70°C decreased elemental sulfur and self-heating in stage B.

5.2 Heat Generating Capacity (HGC) of Samples

The HGC of the samples was investigated through the recycle test procedure (RTP). For most samples, the stage B SHC corresponded with the elemental sulfur generated in each recycle. For the samples conducted at two air flow rates (100mL/min and 300mL/min), the 300mL/min case generated a higher HGC for the Voisey's Bay sample, but a lower HGC for the Sudbury sample.

5.3 Self-heating Reaction Products

Samples from the RTP test were analysed using XRD and XPS. The results showed that with the increasing recycles, the pyrrhotite-related speciesprogressively decreased, being replaced by elemental sulfur, goethite and hydrated iron sulfate products. The observations made on the pyrrhotite and for each product and the possible relationship to self-heating is discussed.

5.3.1 Pyrrhotite

Pyrrhotite was shown to be the primary sulphide that fueled the self-heating reactions (Table 4-4). From literature [48] and the XPS results (Figure 4-30), the pyrrhotite surface is composed of 3 species: polysulphide, monosulphide and disulphide. During the RTP, the composition of the three sulphides changed, as indicated by the XPS peak shift.

Polysulphides appeared to be the most reactive species as evident by their demise during the early stages of oxidation. Monosulphide appeared to be less reactive, and disulphides the least reactive.

5.3.2 Elemental Sulfur

5.3.2.1 Elemental Sulfur Forming Reactions

Elemental sulfur was an intermediate oxidation product that formed in stage A and oxidized in stage B: results showed that the elemental sulfur can be generated

through both the induction (non-self-heating period, as known as delay period) and the self-heating cycles in stage A (Figure 4-19 and Figure 4-20).

Elemental sulfur generation during induction

The induction stage of pyrrhotite oxidation is often defined as the condition where the acid and H_2S formation is inhibited (Section 1.1.3.1, [27]). In this condition, where only moisture and oxygen is provided, elemental sulfur can be generated through the reaction shown in 5.1 [5, 18, 22], "FeS" denoting pyrrhotite:

$$4FeS + 3O_2 + 2H_2O \rightarrow 4FeO \cdot OH + 4S^0 \quad (5.1)$$

Although reaction 5.1 is believed to be exothermic in the self-heating literature [5, 22], the actual heat generated from the reaction has never been experimentally measured [5]. In other pyrrhotite oxidation work [18], this equation was not specifically classified as an exothermic reaction, nor were any temperature increases reported during the experiment [18]. An attempt was made to calculate the enthalpy of the reaction using FactSage; however, due to the lack of information for goethite in the database, the calculation could not be completed.

If the heat generated from reaction 5.1 can be assumed negligible for the particular test conditions (30ºC for Sudbury tailings and 40ºC for Voisey's Bay samples), reaction 5.1 may be responsible for the elemental sulfur generation during the induction period. However, more information is needed in order to evaluate this assumption.

Elemental sulfur generation during self-heating cycles

After induction, when enough acidity and H_2S are released into the system, elemental sulfur is more actively generated (Figures 4-19 and 4-20) through H_2S oxidation [10], as shown in equation 5.2. This reaction has been previously identified as one of the primary reactions responsible for the self-heating in stage A [10].

$$H_2S + \frac{1}{2}O_2 \rightarrow \frac{2}{8}S_8 + H_2O \qquad \Delta H = -2.6\times10^5 \text{ J/mol} \qquad (5.2)$$

5.3.2.2 Elemental Sulfur Formation at Different Airflows

Although it was presumed that a higher air flow rate would generate more elemental sulfur, not all the tests conducted at 300 mL/min generated more elemental sulfur than what was generated at 100 mL/min (Figure 4-11 and Table 4-1).

One of the reasons is that, at highly oxidative conditions, H_2S may oxidize to generate SO_2 (equation 5.3) instead of elemental sulfur, at the same time generating much more heat [10]. The test results support this possibility; the self-heating produced in stage A was always greater at 300 mL/min than at 100 mL/min, although less elemental sulfur was sometimes produced:

$$H_2S_{(g)} + 1½\ O_{2(g)} \rightarrow SO_{2(g)} + H_2O_{(aq)} \qquad \Delta H = -560 \text{ kJ/mol} \qquad (5.3)$$

It is also possible for elemental sulfur to vaporize during stage A, if the sample temperature ever exceeds 95 °C [54]; vaporized elemental sulfur will not be detected by the carbon disulphide method.

5.3.3 Goethite

Goethite is one of the oxidation products formed at the latter stages of oxidation: the XRD results show that goethite is detected after 20 air injections in stage A. From literature [5, 18, 22, 25], goethite is formed through the reactions shown in equations 5.4 and 5.5. The enthalpies of the reactions are not known, however the bi-products of both reactions are known to go through further reactions to generate self-heating. Elemental sulfur generated from reaction 5.4 oxidizes to generate self-heating in stage B, whereas H^+ generated from reaction 5.5 promotes the formation of H_2S, which oxidizes to generate self-heating in stage A.

$$4FeS + 3O_2 + 2H_2O \rightarrow 4FeO \cdot OH + 4S^0 \quad (5.4)$$

$$Fe^{3+}{}_{(aq)} + 2H_2O_{(l)} \rightarrow \alpha FeO \cdot OH + 3H^+{}_{(aq)} \quad (5.5)$$

5.3.4 Hydrated Iron Sulfate

5.3.4.1 Formation of Hydrated Iron Sulfate in Stage A

Hydrated iron sulfate is another oxidation product formed after an extended oxidation period: the XRD results show that hydrated iron sulfate is detected after 7 recycles. From literature [5, 18], hydrated iron sulphate is formed through the reaction 5.6, “FeS” denoting pyrrhotite:

$$FeS + 2O_2 + 7H_2O \rightarrow FeSO_4 \cdot 7H_2O \qquad \Delta H = -9.20\times10^5 \text{ J/mol} \quad (5.6)$$

Previous researchers [9, 18] have noted that the amount of sulphate formed during pyrrhotite oxidation is significantly less than that of goethite or elemental sulfur.

The enthalpy of the reaction at 70ºC was calculated through FactSage. Although the reaction appears to be highly exothermic, it is not expected to be a significant contributor to self-heating reactions, due to the insignificant mass of hydrated iron sulfate found.

5.3.4.2 Dehydration and Rehydration of Hydrated Iron Sulfate

The hydrated iron sulfates may go through dehydration and rehydration, depending on the temperature and moisture present in the system [55-57] (Reactions 5.7 and 5.8). In stage B, where the temperature of the system is raised to 140 ºC, the hydrated iron sulfates dehydrate through the forward reaction. Upon completion of stage B, when the system is cooled back to ambient temperature and moisture is provided, the dehydrated species can re-hydrate through the backward reaction, producing heat of hydration [17, 57].

$$FeSO_4 \cdot 7H_2O \leftrightarrow FeSO_4 \cdot 4H_2O + 3H_2O \qquad (5.7)$$

$$FeSO_4 \cdot 4H_2O \leftrightarrow FeSO_4 \cdot H_2O + 3H_2O \qquad (5.8)$$

The temperature increase observed during re-moisturization (Figures 4-28 and 4-29) were presumed to be the result of the heat of hydration [17]. The as-received samples showed negligible heating upon moisturization, presumably due to the

absence of dehydrated iron sulphates. As the samples went through the RTP, more dehydrated iron sulphates were formed and resulted in higher increases in the sample temperature upon moisturization. The lower temperature increase observed towards the completion of the RTP was presumed to be the effect of more oxidative products forming through the RTP and covering the surface of the iron sulfates, blocking the hydration reaction.

The temperature increase could be a combination of heat of hydration and oxidation of any pyrrhotite left in the sample. The smaller temperature increase observed towards the completion of the RTP can then also be explained by the decrease in pyrrhotite.

5.3.5 General decrease in the bulk Fe and S: ICP Results

The ICP results corresponded with the oxidation results summarized throughout Section 5.3. The decrease in the sulfur content appears to result from the formation of gaseous compounds (such as SO_2 and H_2S) during oxidation, while the decrease in the iron content appears to result from the sample mass increase, through formation of goethite and hydrated iron sulfates [9, 21].

6 Conclusions

The following have been determined from this work:

- The number of air injections in stage A increased the elemental sulfur formation and the self-heating in stage B.
- At 100 mL/min air flow rate, increasing temperature in stage A had mixed results: elemental sulfur formation and self-heating in stage B increased from 40 to 55 ^{o}C but decreased from 55 to 70 ^{o}C. .
- At the higher temperatures the air flow rate of 100 mL/min may have been insufficient for the sulphide sample to fully oxidize.
- Pyrrhotite was identified as the main fuel for self-heating as it disappeared.
- Elemental sulfur, goethite and hydrated iron sulphates were identified as the reaction products of self-heating.
- Elemental sulfur can be generated through both the induction and the self-heating cycles of stage A; it is more actively generated through self-heating cycles.
- Hydrated iron sulphates may go through dehydration and rehydration during the RTP. Dehydrated iron sulphates, when moisturized, generate heat of hydration.

References

1. Prakash, A. and R.P. Gupta, *Surface fires in Jharia Coalfied, India-Their distribution and estimation of area and temperature from TM data.* International Journal of Remote Sensing, 1999. **20**(10): p. 1935-1946.
2. Stracher, G.B. and T.P. Taylor, *Coal fires burning out of control around the world: Thermodynamic recipe for environmental catastrophe.* International Journal of Coal Geology, 2004. **59**(1-2): p. 7-17.
3. Heffern, E.L. and D.A. Coates, *Geologic history of natural coal-bed fires, Powder River basin, USA.* International Journal of Coal Geology, 2004. **59**(1-2): p. 25-47.
4. Good, B.H., *The oxidation of sulfide minerals in the Sullivan Mine.* CIM Bull, 1977. **70**: p. 83-88.
5. Ninteman, D.J., *Spontaneous oxidation and combustion of sulfide ores in underground mines: a literature survey*. 1978, Washington: Dept. of the Interior, Bureau of Mines.
6. Kirshenbaum, N.W., *Transport and Handling of Sulphide Concentrates: Problems and Possible Improvements*, in *Department of Mineral Engineering*. 1967, Stanford University: California.
7. *The Bokuyo Maru*, in *Townsville Daily Bulletin*. 1939, Townsville, Qld: Australia Queensland Townsville.
8. Katayuki, H., *Survey on the Sinking of the N.Y.K. Liner, S/S "Bokuyo Maru".* Journal of the Mining Institute of Japan, 1942. **58**: p. 458-459.
9. Rosenblum, F. and Spira, P., *Evaluation of hazard from self-heating of sulphide rock.* CIM Bulletin, 1995. **88**: p. 44-49.
10. Somot, S. and J. A. Finch, *Possible role of hydrogen sulphide gas in self-heating of pyrrhotite-rich materials.* Minerals Engineering, 2010. **23**: p. 104-110.
11. Somot, S. and J. Finch. *High Self-Heating Rate of a Pyrrhotite-Rich Material: H2S as a Fuel?* in *38th Annual Canadian Mineral Processors conference*. 2006. Ottawa, Ontario, Canada.
12. Farnsworth, D.J.M., *Introduction to and background of sulphide fires in pillar mining at the Sullivan mines.* CIM Bulletin, 1974. **70**: p. 65-71.
13. Rosenblum, F., P. Spira, and K.V. Konigsmann. *Evaluation of hazard from backfill oxidation*. in *International Mineral Processing Congress "Worldwide Industrial Application of Mineral Processing Technology"*. 1982. Toronto, Ontario, Canada: Canadian Institute of Mining and Metallurgy.
14. F. Yang, C.W., Z. Li, *Investigation of the propensity of sulfide concentrates to spontaneous combustion in storage.* Journal of Loss Prevention in the Process Industries, 2011. **24**: p. 131-137.

15. Jung, S., *Sulphide Self-Heating: Moisture Content and sulphur formation*, in *Department of Mining and Materials Engineering*. 2012, McGill University: Montreal, Canada. p. 116.
16. Tributsch, H. and H. Gerischer, *The Oxidation and Self-heating of Metal Sulphides as an Electrochemical Corrosion Phenomenon.* J. Appl. Chem. Biotechnol., 1976. **26**: p. 747-761.
17. Rosenblum, F., J. Nesset, and e. al., *Evaluation and control of self-heating in sulphide concentrates.* CIM Bulletin, 2001. **94**: p. 92-99.
18. Steger, H.F. and L.E. Desjardins, *Oxidation of sulfide minerals, 4. Pyrite, Chalcopyrite and Pyrrhotite.* Chemical Geology, 1978. **23**: p. 225-237.
19. Chen, Y., et al., *Preventing oxidation of iron sulfide minerals by polyethylene polyamines.* Minerals Engineering, 2006. **19**: p. 19-27.
20. Rosenblum, F., J.E. Nesset, and J.A. Finch, *Review of Self-Heating Testing Methodologies*, in *46th Annual Meeting of the Canadian Mineral Processors*. 2014, Canadian Mineral Processors: Ottawa, Ontario, Canada.
21. X. Wang, F.R., et al., *Oxidation, Weight Gain and Self-heating of Sulphides.* The 41st Annual Meeting of the Canadian Mineral Processors, 2009.
22. Wu, C. and Z. Li, *A simple method for predicting the spontaneous combustion potential of sulphide ores at ambient temperature.* Transactions of the Institution of Mining and Metallurgy Section A, 2005. **114**: p. 125-128.
23. Steger, H.F., *Oxidation of sulfide minerals: VII. Effect of temperature and relative humidity on the oxidation of pyrrhotite.* Chemical Geology, 1982. **35**: p. 281-295.
24. Wang, X., *Exploring conditions leading to self-heating of pyrrhotite-rich materials*, in *Mining and Materials Engineering*. 2007, McGill University: Montreal.
25. Janzen, M.P., R.V. Nicholson, and J.M. Scharer, *Pyrrhotite reaction kinetics: Reaction rates for oxidation by oxygen, ferric iron, and for nonoxidative dissolution.* Geochimica et Cosmochimica Acta, 2000. **64**: p. 1511-1522.
26. Nicholson, R.V., R.W. Gilham, and E.J. Reardon, *Pyrite oxidation in carbonate-buffered solution: 2. Rate control by oxide coatings.* Geochimica et Cosmochimica Acta, 1989. **54**: p. 395-402.
27. Belzile, N., et al., *A review on pyrrhotite oxidation.* Geochemical Exploration 2004. **84**: p. 65-76.
28. Dunn, J.G. and L.C. Mackey, *The measurement of the ignition temperatures of commercially important sulfide minerals.* Journal of Thermal Analysis, 1992. **38**: p. 487-494.
29. Iliyas, A., K. Hawboldt, and F. Khan, *Advanced kinetics for calorimetric techniques and thermal stability screening of sulfide minerals.* Thermochimica Acta, 2010. **501**: p. 35-45.

30. Iliyas, A., K. Hawboldt, and F. Khan, *Thermal stability investigation of sulfide minerals in DSC.* Journal of Hazardous Materials, 2010. **178**: p. 814-822.
31. Iliyas, A., K. Hawboldt, and F. Khan, *Kinetics and safety analysis of sulfide mineral self-heating.* J Therm Anal Calorim, 2011. **106**: p. 53-61.
32. Frank-Kamenetskii, D.A., *Diffusion and heat transfer in chemical kinetics*. Second ed. 1969, New York: Plenum Press.
33. Nations, U., *Recommendations on the Transport of Dangerous Goods*. 2011.
34. F. Ferrero, C.L., B.M. Shmidt, M. Noll, M. Malow, *A mathematical model to predict the heating-up of large-scale wood piles.* Journal of Loss Prevention in the Process Industries, 2009. **22**(4): p. 439-448.
35. Nations, U., *Part III Classification procedures, test methods and criteria relating to class 2, class 3, class 4, division 5.1, class 8 and class 9*. 2009.
36. Chen, X.D. and L.V. Chong, *Some characteristics of transient self-heating in an exothermically reactive porous solid slab.* Process Safety and Environmental Protection, 1995. **73**: p. 101-107.
37. Chen, X.D., *On basket heating methods for obtaining exothermic reactivity of solid materials: The extent and impact of the departure of the crossing-point temperature from the oven temperature.* Trans IChemE, 1999. **77**: p. 187-192.
38. Spira, F.R.a.P., *Self-heating of Sulphides.* 13th annual meeting of the Canadian Mineral Processors, 1981: p. 34-49.
39. Ngabe, B., *Estimating activation energy from a sulfide self-heating test.* Minerals Engieering, 2011. **24**(15): p. 1645-1650.
40. Ozdeniz, A.H. and S. Kelebek, *A study of self-heating characteristics of a pyrrhotite-rich sulphide ore stockpile.* International Journal of Mining Science and Technology, 2013. **23**: p. 381-386.
41. Payant, R., *The Self-heating of Sulphide Mixtures*, in *Department of Mining and Materials Engineering*. 2010, McGill University: Montreal, Canada. p. 90.
42. Cruz, R., et al., *An experimental strategy to determine galvanic interactions affecting the reactivity of sulfide mineral concentrates.* Hydrometallurgy, 2005. **78**: p. 198-208.
43. Kwong, Y.T.J., G.W. Swerhone, and J.R. Laurence, *Galvanic sulphide oxidation as a metal-leaching mechanism and its environmental implications.* Geochemistry: Exploration, Environment, Analysis, 2003. **3**: p. 337-343.
44. Abraitis, P.K., et al., *Acid leaching and dissolution of major sulphide ore minerals: processes and galvnic effects in complex systems.* Mineralogical Magazine, 2004. **68**(2): p. 343-351.
45. Gunsinger, M.R., et al., *Evaluation of long-term sulfide oxidation processes within pyrrhotite-rich tailings, Lynn Lake, Manitoba.* Journal of Contaminant Hydrology 2006. **83**: p. 149-170.

46. Bouffard, S.C. and G.D. Senior, *A new method for testing the self-heating character of sulphide concentrates.* Minerals Engineering, 2011. **24**: p. 1517-1519.
47. Payant, R., et al., *The self-heating of sulfides: Galvanic effects.* Minerals Engineering, 2012. **26**: p. 57-63.
48. Pratt, A.R., I.J. Muir, and H.W. Nesbitt, *X-ray photoelectron and Auger electron spectroscopic studies of pyrrhotite and mechanism of air oxidation.* Geochimica et Cosmochimica Acta, 1994. **58**: p. 827-841.
49. Nesbitt, H.W. and I.J. Muir, *X-ray photoelectron spectroscopic study of a pristine pyrite surface reacted with water vapour and air.* Geochimica et Cosmochimica Acta, 1994. 59: p. 4667-4679.
50. Mycroft, J.R., et al., *Detection of sulphur and polysulphides on electrochemically oxidized pyrite surfaces by X-ray photoelectron spectroscopy and Raman spectroscopy.* J. Electroanal. Chem., 1990. 292: p. 139-152.
51. Carlson, T.A., *Photoelectron and Auger Spectroscopy.* 1978: Plenum Press.
52. Wagner, C.D., et al., *Handbook of X-ray Photoelectron Spectroscopy.* 1979: Perkin-Elmer.
53. Jones, C.F., et al., *Compositional and structural alteration of pyrrhotite surfaces in solution: XPS and XRD studies.* Appl. Surf. Sci., 1992. 55: p. 65-85.
54. Bojes, J., J. Lerbscher, and W. Wamburl, *Elemental Sulfur in 3-phase Sour Gas Systems - Is condensate really your Ally?*, in *Northern Area Western Conference*. 2010, NACE International: Calgary, Alberta.
55. Wang, T., K.A. Debelak, and J.A. Roth, *Dehydration of iron (II) sulfate heptahydrate.* Thermochimica Acta, 2007. **462**: p. 89-93.
56. Wang, A., et al., *Stability field and phase transition pathways of hydrous ferric sulfates in the temperature range 50C to 5C: Implication for martian ferric sulfates.* Icarus, 2012. **218**: p. 622-643.
57. Clark, B.C., *Implications of Abundant Hygroscopic Minerals in the Martian Regolith.* Icarus, 1978. **34**: p. 545-605.